Technologies to Enhance Operation of the Existing Natural Gas Compression Infrastructure

Quarterly Technical Progress Report

Reporting Period Start Date: 07/01/04
Reporting Period End Date: 09/30/04

Principal Authors:

Anthony J. Smalley
Ralph E. Harris
Gary D. Bourn

October 2004

DOE Award No. DE-FC26-02NT41646
SwRI Project No. 18.06223

Submitting Organization:

Southwest Research Institute®
6220 Culebra Road
San Antonio, TX 78238-5166

DISCLAIMER

"This report was prepared as an account of work sponsored by an agency of the United States Government. Neither the United States Government nor any agency thereof, nor any of their employees, makes an warranty, express or implied, or assumes any legal liability or responsibility for the accuracy, completeness, or usefulness of any information, apparatus, product, or process disclosed, or represents that its use would not infringe privately owned rights. Reference herein to any specific commercial product, process, or service by trade name, trademark, manufacturer, or otherwise does not necessarily constitute or imply its endorsement, recommendation, or favoring by the United States Government or any agency thereof. The views and opinions of authors expressed herein do not necessarily state or reflect those of the United States Government or any agency thereof."

ABSTRACT

This quarterly report documents work performed under Tasks 10 through 14 of the project entitled: *Technologies to Enhance Operation of the Existing Natural Gas Compression Infrastructure*. The project objective is to develop and substantiate methods for operating integral engine/compressors in gas pipeline service, which reduce fuel consumption, increase capacity, and enhance mechanical integrity. The report documents the second series of tests performed on a GMW10 engine/compressor after modifications to add high pressure Fuel and a Turbocharger. It also presents baseline testing for air balance investigations and initial simulation modeling of the air manifold for a Cooper GMVH6.

TABLE OF CONTENTS

Page

LIST OF FIGURES

Page

LIST OF FIGURES (*CONTINUED*)

Page

LIST OF FIGURES (*CONTINUED*)

Page

LIST OF FIGURES (*CONTINUED*)

Page

LIST OF TABLES

Page

1. INTRODUCTION

This report presents results from a series of tests performed on an GMW10 integral engine compressor in natural gas transmission service, installed at Williams' Station 60 (St. Francisville station). This is the second series of tests on this engine, and provides data to compare performance of this engine after modification (including addition of high-pressure fuel and a turbocharger) with previously measured performance prior to these modifications. The report also presents results from air balance testing and modeling.

1.1 THE US GAS TRANSMISSION COMPRESSION INFRASTRUCTURE

The gas transmission industry operates over 4000 integral engine compressors, which play a major role in pumping natural gas through the US pipeline system. Although the use of centrifugal compressors in the US pipeline industry has grown, these integral reciprocating units still represent over 70% of the fleet in numbers, and over half the installed power. These "slow-speed" integral engine compressors have been the workhorses of the industry for over 50 years, providing the reliable gas compression needed by the pipeline system. Figure 1-1 shows two such units: a 48-year old TLA6 and a 50-year old GMW10.

Figure 1-1. TLA6 (2000 HP) and GMW10 (2500 HP) in Pipeline Service

Figure 1-2 shows the age distribution of the current infrastructure. Over half the fleet is well over 40 years old, but replacing all these units with currently available technology would incur a huge cost and disruption to service with insufficient improvement in overall performance of the pipeline system to justify this cost and disruption. For these reasons, wholesale replacement remains unlikely (although selective replacement driven by factors such as environmental regulations can be expected). Growth to a 30-TCF-plus gas market in the US, anticipated over the next 10 to 20 years, must come on the backs of the existing compression infrastructure; it will, therefore, depend on continued integrity, enhanced capacity, and efficiency of the existing integral engine/compressors under all loads. The industry needs demonstrated technology options and operating methods, which will cost-effectively maximize the capacity of these old units, and reduce their fuel consumption, while respecting or improving their integrity.

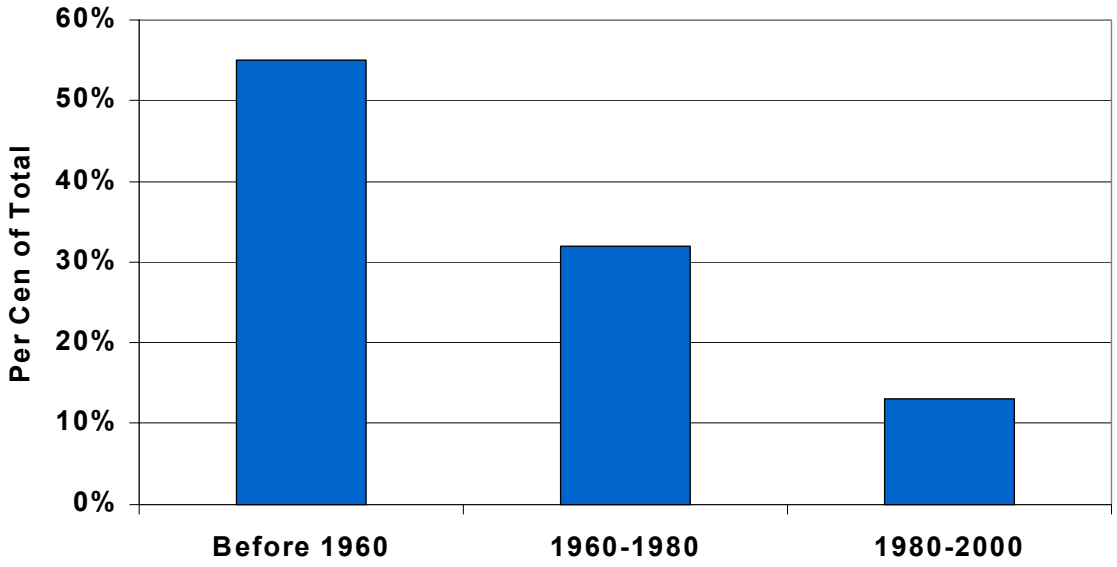

Figure 1-2. Install Dates: Over 50% of Pipeline Compressors Exceed 40 Years Old

Figures 1-3, 1-4, and 1-5 exemplify these needs of the existing infrastructure.

Figure 1-3 shows how annual fuel consumption at individual compressor stations in the pipeline system varies with the number of horsepower hours delivered by the engine to the compressor cylinders at that station. Points on the high side of the mean slope represent stations which are burning more than the industry average. In addition, with a regressed slope of 7.7 CF/BHP-hr. for Figure 1-3, the industry burns significantly more fuel than the most efficient current technology natural gas engines (as little as 6 CF/BHP-hr.). As a slightly different performance measure for the industry, Smalley et al [1] calculate an industry average (ratio of total fuel volume to total BHP-hours) of 8.25 SCF/BHP-hr.

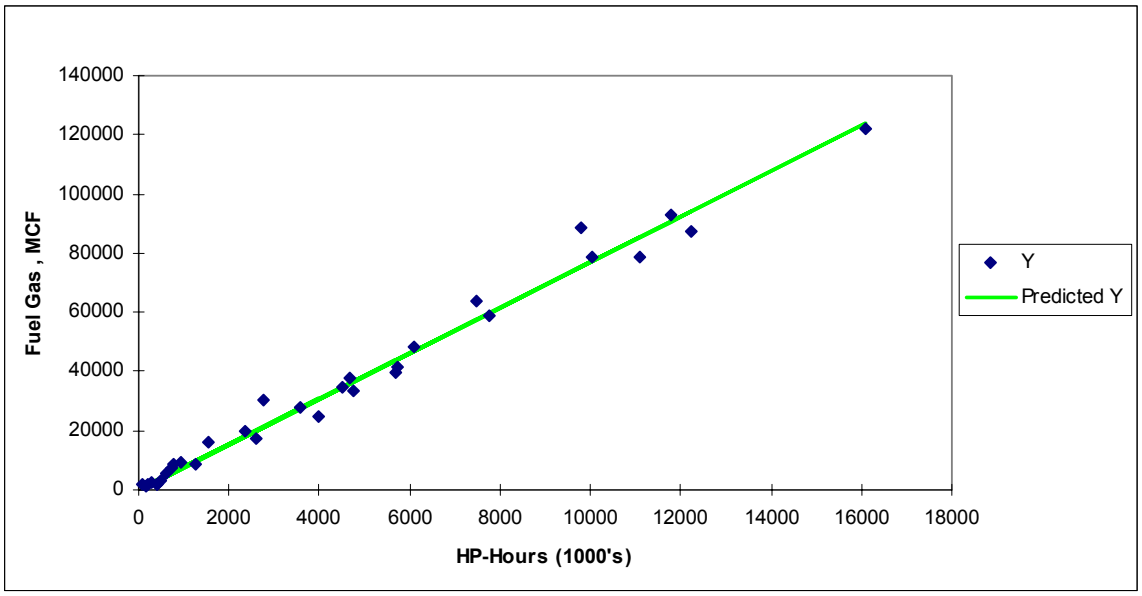

Figure 1-3. Industry Fuel Consumption
(~7.7 MCF/HP-Hr. +/-20% - Need to Lower the High Values)

Figure 1-4 presents a distribution of compressor thermal efficiency for the industry created by GMRC from a quantitative survey a number of years ago. This is the efficiency with which the compressors convert HP-hours to useful compression. The width of the range and the 12 points by which the 79% median lies below the best achieved (91 to 92%) represents not only gas which is burnt rather than delivered, but also engine capacity which must overcome losses rather than deliver useful compression of the transported gas.

Figure 1-5 shows a number of failed crankshafts. This problem continues to occur at an undesirable rate for the pipeline industry as a whole (about one failure per thousand engines per year). This rate may not seem excessive, but for the compressor station and company which incurs such a failure, the disruption, cost, and loss of capacity at the time is significant. The chance of this rate increasing as a penalty for improved performance and increased capacity must be avoided, as well as any increase in problems such as bearing failure, or damage caused by detonation, or unintended overload.

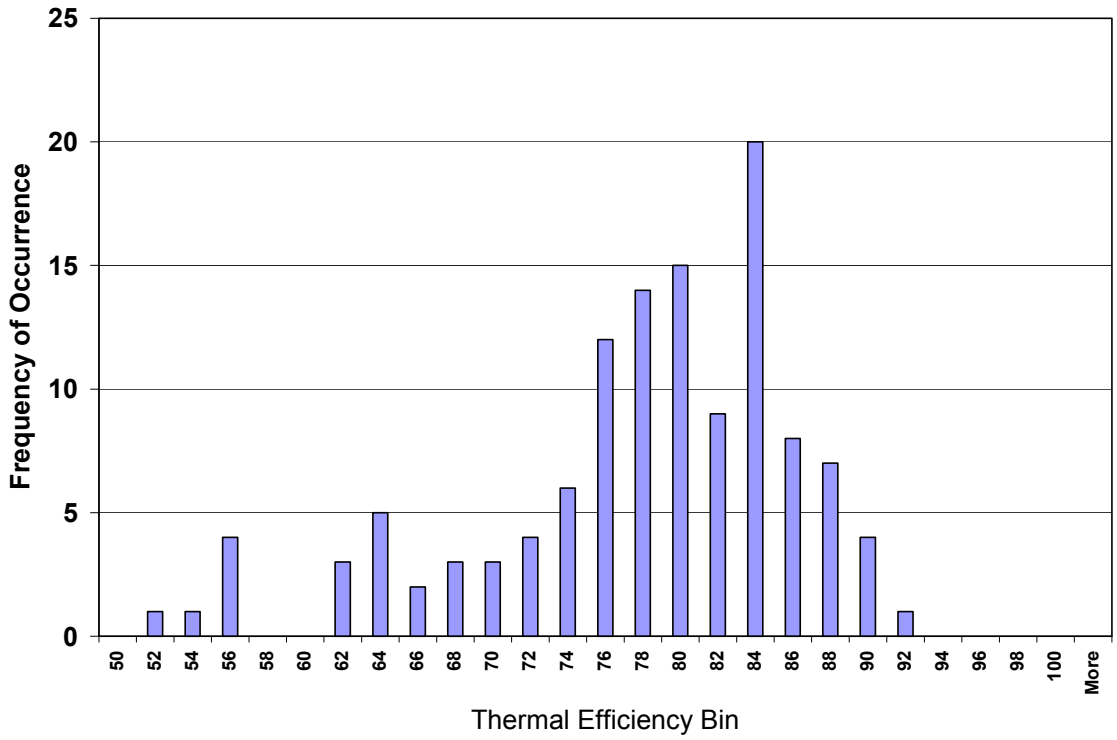

Figure 1-4. Compressor Thermal Efficiency Histogram based on GMRC Survey

Figure 1-5. Integrity: Crankshaft Failure Examples – Need Methods of Avoidance

1.2 THE COMPRESSION INFRASTRUCTURE PROJECT

Three years ago, the US Department of Energy (DOE) initiated a Natural Gas Infrastructure (NGI) program, whose goals include increasing capacity of the current pipeline infrastructure (10%), and reducing operational costs (50% by 2010). As a part of this program, SwRI is undertaking a project entitled "Technologies to Enhance the Existing Natural Gas Compression Infrastructure". The project is managed for DOE by the National Energy Technology Laboratory (NETL). The project objective is:

> To develop and substantiate methods for operating integral engine/compressors in gas pipeline service which reduce *fuel consumption*, increase *capacity*, and enhance mechanical *integrity*.

1.3 PROJECT ACCOMPLISHMENT

This project continues to document and demonstrate feasibility of technologies and operational choices for companies who operate the large installed fleet of integral engine compressors in pipeline service. Applying project results will enhance integrity, extend life, improve efficiency, and increase capacity, while managing NOx emissions. These benefits will translate into lower cost, more reliable gas transmission, and options for increasing deliverability from the existing infrastructure on high demand days. In the process, the project has assembled a powerful suite of

instruments and a data system, with which it has characterized behavior of the units tested under a wide range of conditions. This suite will remain available for characterization and optimization after completion of the project. At the project mid-point, the following documents its ongoing value and contribution to DOE goals.

1.3.1 INTEGRITY

Increasing integrity and reducing statistical likelihood of component failure reduces transmission cost and enhances aggregate deliverability. Detonation represents a damaging threat to an engine. Applying the detonation detection technology tested under the project will mitigate this threat, which widely inhibits potentially beneficial operation with advanced timing. The newly defined CPR balancing method, which has proved quick and convenient to apply, will help equalize air fuel ratio across cylinders and reduce the tendency to detonate. The low cost control method demonstrated for maintaining a global equivalence ratio set point provides another option for maximizing margin between misfire and detonation limits, using commercially available controllers. The crank strain data capture module (SDCM) applied on all engines tested has shown its value for defining conditions when crank damage rate increases. Measuring crankshaft torsional velocity has complemented the SDCM, particularly in documenting the influence of speed changes, showing also that torsional velocity data responds detectably to loss of torque from a misfire. The rod load monitor evaluated and enhanced on every test so far promises to avoid overload of engines and resulting damage, by improving consistency of load torque values used in load step control.

1.3.2 EFFICIENCY

As much as 3% of the natural gas consumed goes as fuel gas for engines and turbines to drive compressors. This fuel gas would cost $3 billion at current - the single most significant cost of gas transportation. Increasing the aggregate efficiency with which engine/compressors convert fuel energy into useful compression work will reduce this cost and leave more of the gas in the pipeline system available to the end user. The project has already documented how high-pressure fuel injection coupled with addition of a turbocharger on old GMW engines reduces heat rate by about 7%. The rod load monitor discussed above will allow engine operation at the

point of highest efficiency (100% torque), with greatly reduced risk of overload. The detonation detector will safely allow more efficient engine operation with timing advanced. Comparison with the heat rate *versus* load characteristic has revealed small potential benefits in brake thermal efficiency by applying CPR balancing. Project mapping of system efficiency has made clear the importance of considering both compressor and engine when evaluating how operational decisions will impact fuel conversion efficiency; speed/load combinations which favor heat rate may at the same time hurt compressor efficiency, so that maximizing efficiency requires careful choices based on data. The project will continue to identify ways to enhance this efficiency, with emphasis on the compressor and pulsation control. The limitations in relying on differential indicated power for compressor efficiency calculations has emphasized the need for an effective method of measuring compressor flow and temperature rise, and the project will start evaluating alternatives. The project has also made clear the need for more information about mechanical losses and will seek to add to this knowledge with new interpretation of the rod load data. Valve leaks represent a significant loss of compressor efficiency system-wide. Engine/compressor operators know the sensitivity of temperature rise to valve leaks, but the project has re-emphasized this sensitivity; the data normalization and statistical process control techniques already promoted by McKee, et al [2] would lend themselves very effectively to monitoring of cylinder temperature rise and associated decision making based on economic significance. The project has documented air imbalance between cylinders as a widespread condition that can limit combustion efficiency; new tasks will characterize air imbalance in more detail and seek cost-effective solutions.

1.3.3 CAPACITY

As discussed above, integrity enhancement and reduced component failure probability will enhance aggregate deliverability. In addition to improving the efficiency of fuel conversion, all increases in compressor efficiency will reduce the fraction of available engine power that must go to overcome losses, and will thereby also add to deliverability. Tests so far have shown a compressor efficiency range from 84% to 91%, adding to an earlier GMRC survey with a range from 52 to 92%! The high compressor efficiency values found present a benchmark that will add greatly to system capacity if more widely achieved. The remainder of the project will seek to re-emphasize compressor efficiency by characterizing and reducing compressor losses, both

mechanical and thermodynamic. Measurements of flow, temperature rise, and dynamic pressure in the cylinder nozzles (as well as in the cylinders themselves) will help quantify and characterize inherent thermodynamic losses – a first step in their reduction. Previous tests have shown the likely contribution of pulsations to these losses, yet pulsation control methods such as acoustic filters and orifices must take account also of associated resistive pressure losses.

1.4 FIELD TEST PROGRAM OVERVIEW

The tests and analyses have been performed so far on two different two-stroke engine models from two manufacturers: a Cooper GMW10 with three compressor cylinders, and a Dresser-Clark HBA-6T with four compressor cylinders. The HBA is a straight six with turbocharger. The GMW is a V-10, and has been tested both with and without the combination of a turbocharger and high-pressure fuel injection system. The engine selection was based on detailed quantitative analysis of the engine population using a database prepared for the pipeline industry, which shows both models are in the top six, measured by horsepower installed or by number of units installed. Thus, marked diversity has been achieved in the process of testing two widely deployed engine models. This quarterly report focuses on results from a second series of tests on a specific GMW10 (Unit 6) at Williams' Station 60 (St. Francisville, Louisiana). The first test series established performance in original condition. The tests reported here present performance after modification to add high-pressure fuel and a turbocharger.

The data obtained includes:

- Performance of engine (heat rate and normalized NOx) as a function of timing, speed, and torque.
- Performance of compressor as a function of speed and load step.
- System efficiency as a function of speed, timing, and load.
- Crankshaft strain as a function of balance condition, load, and timing.
- Comparison of rod load monitor output with indicated cylinder power.
- Correlation of detonation detector output with audible detonation and peak-firing pressure.

- Further demonstration of CPR balancing and how it influences average and instantaneous spread in peak-firing pressure and combustion pressure ratio.

Plans are now underway to test a four-stroke 10KVG3 at Duke's Thomaston station in South Texas in early November.

2. EXPERIMENTAL

2.1 SENSORS AND DATA CHANNELS FOR FIELD MEASUREMENT

Sensors and data acquisition capability have been assembled to record the following data on large integral engine compressors in the field.

- *Dynamic Pressure in the Compressor Cylinders* – these measurements are used for compressor horsepower and flow determination. Both ends of each compressor cylinder have been instrumented for dynamic pressure in each test series. The sensors are Sensotec piezo-restrictive transducer). They are calibrated prior to each test by deadweight loading to generate known force per unit area in the test fluid applied to the sensing element.

- *Dynamic Pressure in the Engine Cylinders* – these measurements are used for engine horsepower determination, engine balancing, and to calculate engine statistics. All power cylinders have been instrumented for dynamic pressure in each test series. The sensors are Kistler quartz piezoelectric transducers. Being dynamic sensors, they are calibrated prior to each test by suddenly applied deadweight loading to generate known force per unit area in the test fluid applied to the sensing element.

- *Dynamic Pressure in the Engine Air Intake Manifold* – these measurements are used to correlate dynamic effects in the manifolds, which deliver air for each cylinder with the dynamic statistics within each cylinder. They also provide the time-averaged value for air manifold pressure whose influence on engine heat rate and emissions is assessed. Air manifolds have been instrumented in each test series. The sensors are Kistler piezo-resistive pressure transducers with factory provided calibration.

- *Dynamic Pressure in Engine Exhaust* – these measurements are used to determine dynamic variation of pressure in the manifolds, which capture hot exhaust gas from each cylinder, and to correlate these dynamic pressure variations with the dynamics within each cylinder. The sensors are Kistler piezo-resistive transducer with factory provided calibration; they are water-cooled to reduce uncertainty resulting from temperature influence on the sensor readings.

- *Torsional Vibrations (IRV)* – This measures the dynamic variation in speed of rotation of the flywheel. The sensor is a BEI 512 pulse encoder driven through a flexible coupling by a shaft connected by a friction drive to the flywheel. The frequency of its output pulse train directly reflects instantaneous flywheel angular velocity, which varies within each cycle of the engine as a result of dynamic load variation. Rather than digitally time the variation in period between pulses (which imposes unrealistic period discrimination requirements), a frequency to voltage analog circuit is used to determine the continuous variation in flywheel speed. The speed variation is assessed as a surrogate for mechanical integrity. The frequency-to-voltage measurement is calibrated by supplying the analog circuitry with a pulse train of known frequency from a signal generator. The torsional vibration has been measured in this way on all tests. The torsional vibration data has been assessed as a potential indicator of engine dynamic loading severity.

- *Data Acquisition Triggering* – The BEI encoder signal is also used to trigger acquisition of samples from all dynamic transducers. The phasing of the pulse train to top dead center is important. A pre-established top dead center mark for power Cylinder 1 is used as a reference, and the angular setting within the DAS corresponding to Cylinder 1 TDC is adjusted, as the engine runs, until a strobe light triggered by the DAS at this angle shows the mark on the flywheel coincides with the stationary mark.

- *Bearing Centerline Vibration* – This measurement is assessed as an indicator of engine dynamic loading severity. The sensors are PCB velocimeters with factory provided calibration. The sensors have been located to measure lateral vibration at each end of the engine/compressor frame.

- *Crankshaft Dynamic Strain* – This measurement is used as a direct indicator of shaft loading, and to provide a link between engine statistical quantities and potential for crankshaft fatigue damage [3]. The strain gage is placed on the crankshaft web as close as possible to the crank pin – at the point most sensitive to opening and closing of the crank throw faces under load from engine and compressor rods. Data is acquired by the Strain Data Capture Module (SDCM), which rides on the shaft within the engine during each day of testing, and from which data is downloaded at the end of each day. This is calibrated using a calibration resistance. The SDCM has worked with complete reliability for all tests so far.

- *Engine Fuel Flow* – Used to document overall engine efficiency. The sensor is an Emerson Flobas 103 transmitter which implements the AGA3 flow measurement based on a differential pressure measurement, and is factory calibrated with a certificate. This sensor is connected to taps on the already installed engine fuel flow orifice, which has been available on all engines tested so far. The fuel flow, coupled with a gas analysis, provides the basis for determining fuel energy consumed by the engine, and for determining heat rate and overall system efficiency. At the first test, the flow measurement functioned, but the flow range was not properly matched to the engine, and satisfactory data was not obtained. At subsequent tests, the fuel flow has been successfully measured and used for the intended purposes.

- *Suction Header and Discharge Header Pressures and Temperatures* – These measurements are used for installation efficiency determination. Pressures are measured with Sensotec piezo-restrictive transducers.

- *Engine Exhaust O_2 Level* – This measurement is used to determine global equivalence ratio, both as an independent variable influencing engine performance, and where the loop is closed to the turbocharger waste-gate for active control. The sensor used is an NGK fast-response transducer, which provides a continuous variation of voltage with exhaust oxygen level. It is calibrated against a standard.

- *Engine Exhaust NOx Level* – This measurement is used to provide comparative emissions data. The sensor used is an NGK fast-response transducer, which provides a continuous variation of voltage with exhaust NOx level. It is calibrated against a standard.

- *Compressor Rod Load* – This measurement is used for both mechanical integrity and loading optimization. The sensor uses a pair of strain gages mounted on either side of the rod, which are bridged additively to cancel bending and produce a signal proportional to axial load on the piston rod. The signal is transmitted using RF from a moving antenna to a stationary antenna. The strain gage and signal transmission can be powered by a battery, or by a generator driven by rod motion. The battery power is adequate and simpler to set up for short-term tests, but for continuous monitoring and control self-powering is needed. Calibration issues are not fully resolved yet for this device (termed the "rod load monitor" (RLM)). So far, the horsepower measurement from the compressor cylinder, based on cylinder pressure transducer, has been used for calibration.

- *Knock Detection* – Evaluation of a sensor provided by Metrix, which counts occurrences of dynamic acceleration levels above a threshold.

2.2 LABORATORY GMVH MEASUREMENTS FOR AIR BALANCE TASK

The GMVH engine was highly instrumented prior to utilization for the air balance investigation. However, additional dynamic pressure measurements were required for proper simulation with the computational model. The additional instrumentation is as follows:

- *Dynamic Pressure in Exhaust Manifold Runners* – Prior to the air balance investigation, only Cylinder 1L was instrumented for dynamic exhaust pressure. Additional dynamic pressure sensors were added to the remaining five cylinders to capture the dynamic pressure pulsations of the exhaust from each cylinder's ports. These sensors are of a thin-film strain gage type, typically used for absolute pressure measurement of manifold pressure in automotive electronic engine control systems. Each sensor was calibrated and a comparison

test to a Kistler piezo-resistive sensor was performed on the running engine to validate transient response.

- *Dynamic Pressure in Exhaust Manifold Plenum* – A new sensor was installed in the exhaust manifold plenum near the turbocharger. This measurement is required to capture the dynamic pressure pulsations in the exhaust manifold plenum and provide data to characterize the dynamic flow through the exhaust manifold. A Kistler piezo-resistive absolute pressure transducer was utilized for this measurement. This sensor was calibrated via a deadweight tester. A photograph of the exhaust plenum sensor, as installed for testing, is provided in Figure 2-1.

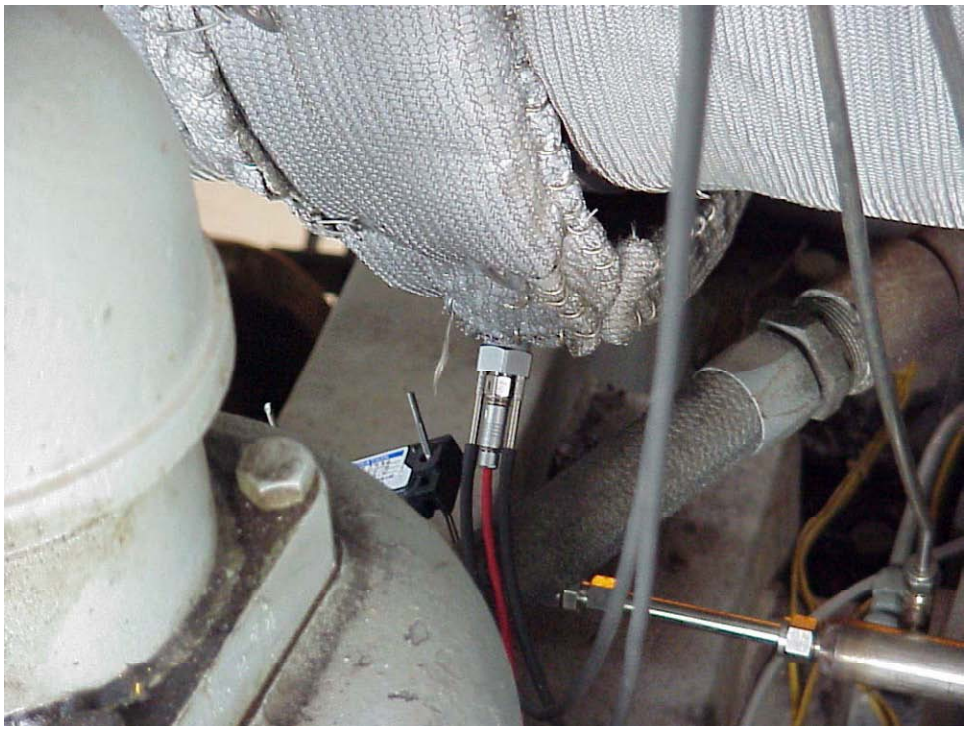

Figure 2-1. Photograph of Dynamic Exhaust Pressure Sensor in Exhaust Plenum

- *Dynamic Pressure in Inlet Manifold Plenums* – Prior to the air balance investigation, only the left inlet manifold was instrumented for dynamic inlet plenum pressure. An additional dynamic pressure sensor was added to the right inlet manifold plenum to capture the dynamic pressure pulsations of the exhaust from each cylinder's ports. These sensors are of a thin-film strain gage type, like those utilized in the exhaust manifold runners.

The complete instrumentation package on the laboratory GMVH engine is listed in Table 2-1.

Table 2-1. Time-Averaged and Crank-Angle Resolved Measurements on GMVH

Time-Averaged Measurements	
Engine Speed	Oil Pressure
Turbocharger Shaft Speed	Turbocharger Oil Pressure
Turbocharger Wastegate Position	Coolant Inlet & Outlet Pressure
Engine Torque	Pre-Turbine Pressure
Total Fuel Flow	Stack Pressure
Pre-Chamber Fuel Flow	Compressor Inlet Temperature
Fuel Gas Composition	Compressor Left & Right Outlet Temperatures
Fuel Gas Heating Value	Inlet Manifold Left & Right Temperatures
Total Air Flow	Fuel Header Temperature
Barometric Pressure	Pre-Chamber Header Temperature
Ambient Temperature	Individual Cyl. Exhaust Runner Temperatures
Ambient Humidity	Pre-Turbine Temperature
Exhaust NOx Concentration	Post-Turbine Temperature
Exhaust CO Concentration	I/C Inlet Left & Right Water Temperatures
Exhaust HC Concentration	I/C Outlet Left & Right Water Temperatures
Exhaust CO2 Concentration	Oil Sump Temperature
Exhaust O2 Concentration	Oil Inlet Temperature
Exhaust Equivalence Ratio	Turbocharger Oil Inlet Temperature
Inlet Manifold Left & Right Pressures	Coolant Inlet & Outlet Temperatures
Fuel Header Pressure	Individual Cyl. Head Temperatures
Pre-Chamber Header Pressure	Dynomometer Inlet & Outlet Temperatures
Crank-Angle Resolved (Dynamic) Measurements	
Cylinder 1L Firing Pressure	Cylinder 1L Exhaust Runner Pressure
Cylinder 2L Firing Pressure	Cylinder 2L Exhaust Runner Pressure
Cylinder 3L Firing Pressure	Cylinder 3L Exhaust Runner Pressure
Cylinder 1R Firing Pressure	Cylinder 1R Exhaust Runner Pressure
Cylinder 2R Firing Pressure	Cylinder 2R Exhaust Runner Pressure
Cylinder 3R Firing Pressure	Cylinder 3R Exhaust Runner Pressure
Left Inlet Manifold Plenum Pressure	Right Inlet Manifold Plenum Pressure
Cylinder 1L Pre-Chamber Firing Pressure	Exhaust Manifold Plenum Pressure

In addition to the many measurements for engine performance and emissions, several static measurements are being made of the engine geometry. These geometric measurements have been determined to be of critical importance for proper simulation of the engine. The key geometric parameters to be determined are compression ratio, port timing, and port flow coefficient *versus* open area for each cylinder of the test engine. In order to conduct the many detailed measurements, the engine has been disassembled.

Two of the six cylinders, representing a high and low compression pressure, will be flow tested. The flow testing will be conducted to measure the discharge coefficient of both intake and exhaust ports *versus* open area. Accurate discharge coefficients are required for accurate simulation. This data is not readily available, therefore, measurement is required. In addition, a review of allowable port shape on the manufacturing drawings has given concern that variance in port shape from cylinder-to-cylinder could be a large contributor to flow imbalance. This flow test of a high and low flow cylinder will allow the affect to be characterized and account for in the simulations.

2.3 COMPUTATIONAL MODELING FOR AIR BALANCE INVESTIGATION

The computational modeling for the air balance investigation is being performed with software purchased from Optimum Power Technology. The particular software package is titled *Automated Design with Virtual 2-Stroke*. This software is a one-dimensional cycle-simulation model that focuses on the fluid dynamics in an internal combustion engine.

3. DATA ACQUISITION

3.1 FIELD DATA SYSTEM

Figures 3-1 and 3-2 show photographs of the Data Acquisition System (DAS). The system comprises an industrially hardened computer, a flat screen for display, and a separate box with connectors to which cables from individual sensors are connected. The DAS box has analog-to-digital converters of appropriate speed for over 50 different channels.

The individual power cylinder transducers (up to 10) are connected to a box with connectors on the deck near the cylinders. A single cable from this box carries the signals from all the power cylinder transducers to the main data acquisition box. A similar approach is used for the compressor cylinders. In this way, the complexity of the cabling and system checkout is minimized. Signals from rod load monitors, from other system pressures, and from temperature sensors are acquired by the DAS; concurrently, and a database of the sensor values throughout each test is created by the DAS.

3.2 LABORATORY GMVH ENGINE

A photograph of the laboratory GMVH instrumentation and control panel is depicted in Figure 3-3 below. The data acquisition system is PC-Based, and features custom software written by SwRI. In addition to recording and displaying the measurements listed in Section 2-2, the data acquisition software is programmed with many calculated parameters that are displayed in real-time for monitoring performance and setting specific operating conditions.

Figure 3-1. Front View of Data Acquisition System (DAS)

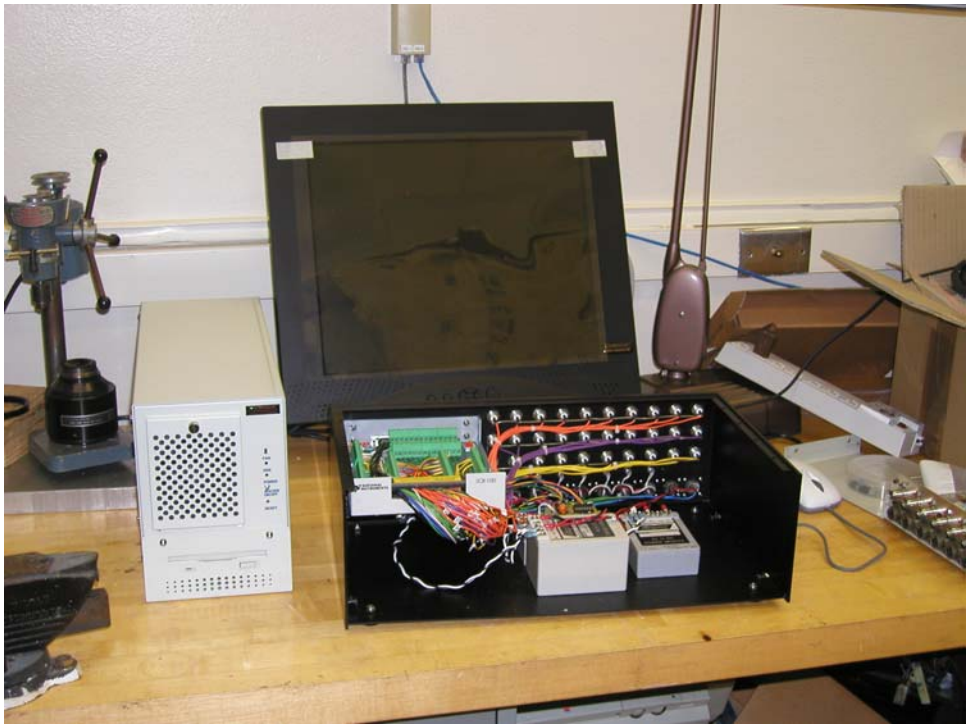

Figure 3-2. Rear View of Data Acquisition System (DAS)

Figure 3-3. Laboratory GMVH Instrumentation and Control Panel

4. RESULTS AND DISCUSSION: TEST OF MODIFIED GMW10

4.1 OVERVIEW

This section presents results from tests on a GMW10 at Williams' Transco's Station 60 at St. Francisville in Louisiana, performed August 2004. These are the second set of tests on Unit 6 at this station, performed after the unit was modified to incorporate high-pressure fuel (Enginuity's HPFI™ system) and a turbocharger. An earlier set of tests in February 2004 established performance prior to these modifications.

All instrumentation except the exhaust manifold dynamic pressure sensor was installed, including the detonation detector.

4.2 TYPICAL WAVEFORMS

Figures 4-1, 4-2, and 4-3 show typical waveforms from the ten power cylinder pressure transducers, from the six compressor cylinder ends, and from the rod load monitor, respectively. Each of these represent time series averaged data as a function of crank angle. The power cylinders show some cylinder-to-cylinder variation in peak-firing pressure, with a spread from minimum to maximum of 64 PSI (about 13%). The compressor cylinders are more consistent in their peak pressure values. The rod load data reflects the difference between head and crank end forces, including pressure, inertia, and friction. The higher frequency modulation in the signal is an artifact of the magnet array, which provides excitation for the moving coils.

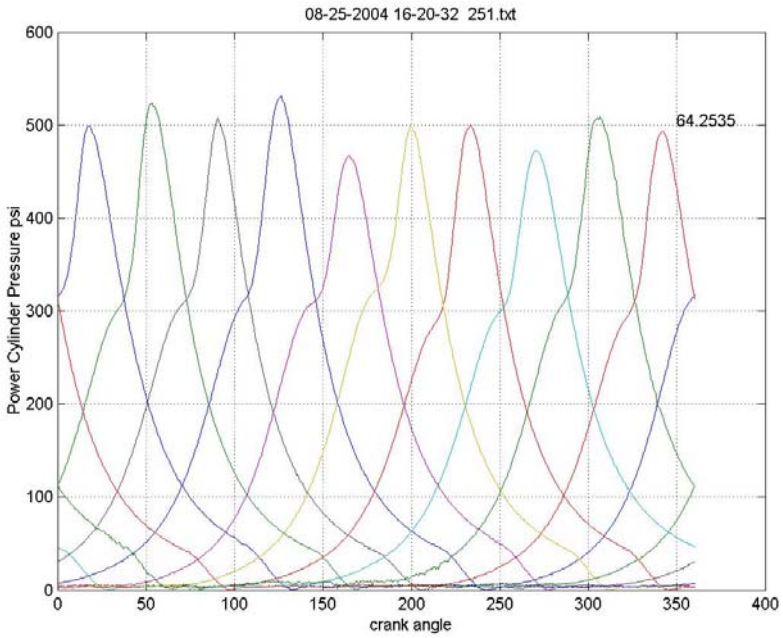

Figure 4-1. Representative Pressure Data for Ten Power Cylinders; Williams' Station 60; GMW10, Unit 6; After Modifications; Day 1; August 25, 2004

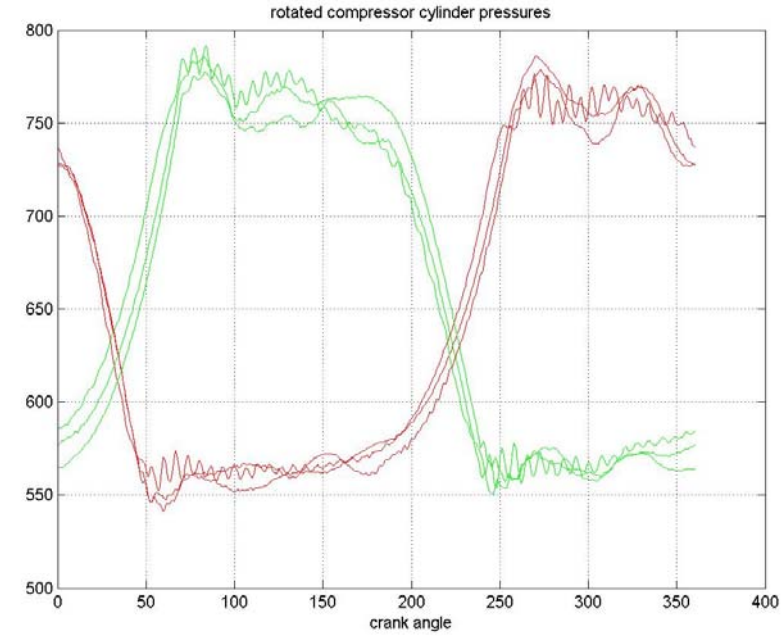

Figure 4-2. Representative Pressure Data for Head and Crank End of Three Compressor Cylinders; Williams' Station 60; GMW10; Unit 6; After Modifications; Day 1; August 25, 2004

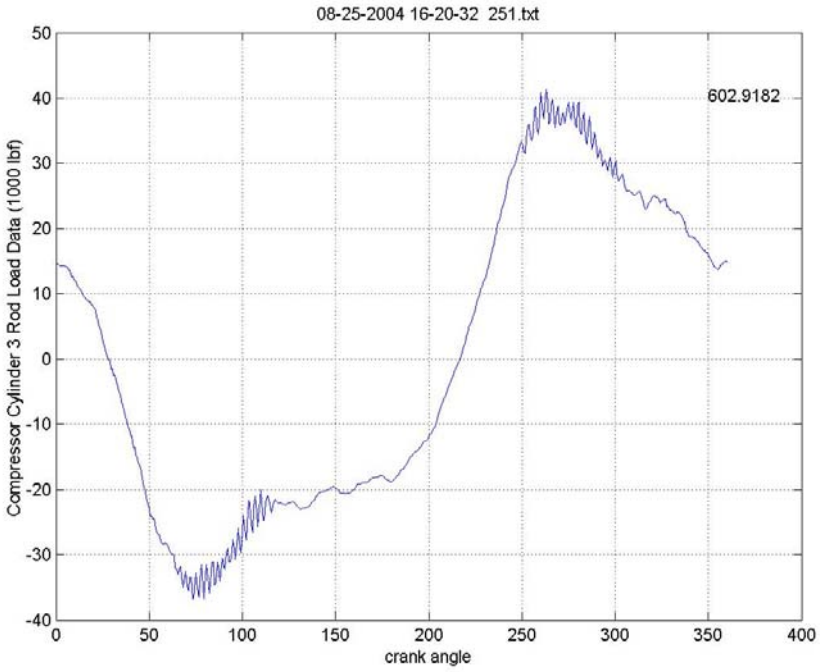

Figure 4-3. Representative Data from Rod Load Monitor (Thousands of Pounds Force); Williams' Station 60; Day 1; GMW10; Unit 6; After Modifications; August 25, 2004

4.3 SPEED VARIATION

Figure 4-4 shows the speed variation during Day 1 of the two-day test. For this first day's testing, speed was kept constant at 250 RPM; small differences from 250 RPM were generally 1 RPM or less, and just reached 2 RPM for a short period around 14:50. Figure 4-5 shows the speed on Day 2 was also maintained close to 250 RPM most of the day, but was intentionally varied down to 237 RPM, and then to 225 RPM between 13:50 and 15:10.

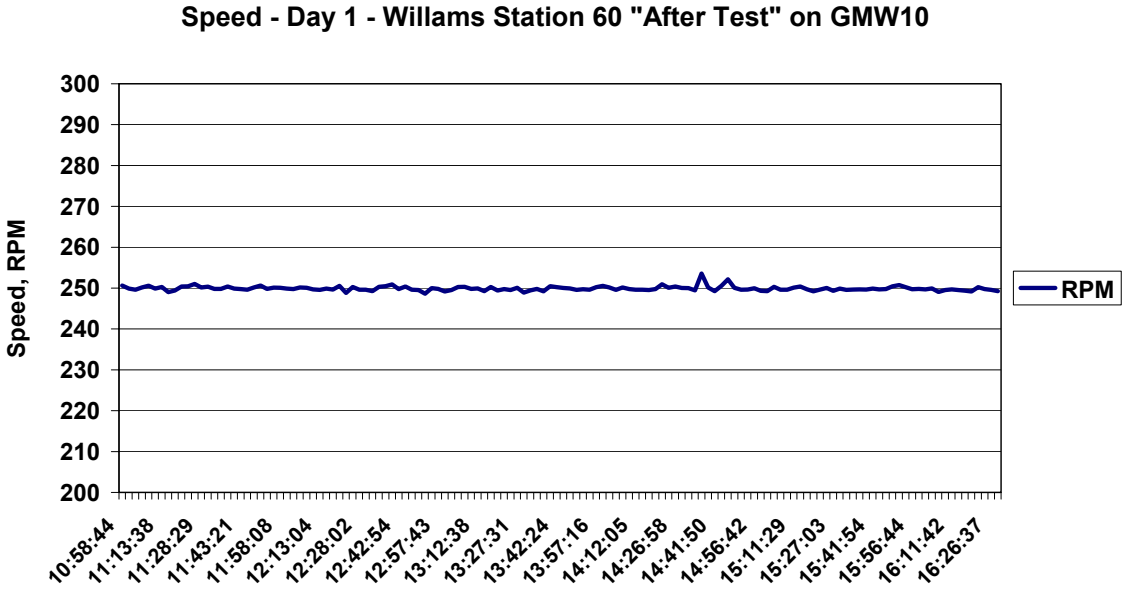

Figure 4-4. Speed; Day 1 Tests; Williams' Station 60; GMW10; Unit 6; After Modifications; August 25, 2004

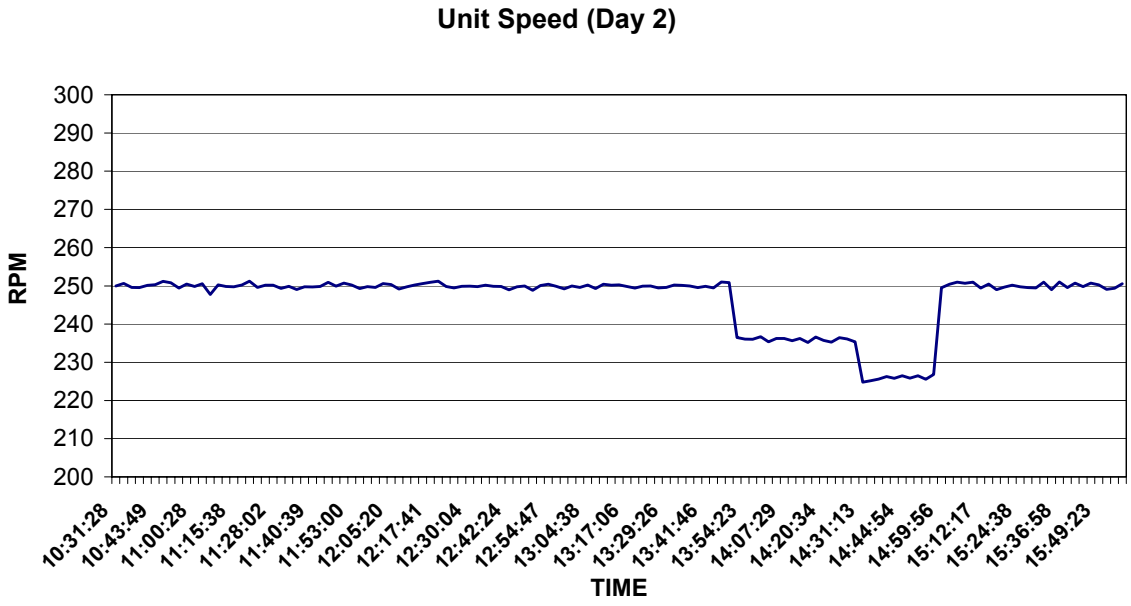

Figure 4-5. Speed; Day 2 Tests; Williams' Station 60; GMW10; Unit 6; After Modifications; August 26, 2004

4.4 HEAT RATE

Figure 4-6 shows the engine heat rate varied during the first day's testing from a minimum of 6800 BTU/HP-hr. to 7050 BTU/HP-hr. The quantities varied on this day, which influenced the heat rate, are shown in Figure 4-6 to be timing and load step, which influenced torque. The data indicates that retarding timing from its initial value of 9 degrees BTDC back to 6 degrees (at 96 to 97% torque) increases heat rate from an average of about 6810 to an average of about 7040. The value at 8 degrees is about 6890. The data also shows that decreasing torque from between 96 and 97% to 88% increased heat rate from 6810 to 6950 BTU/HP-hr. The comparable numbers at a torque of 102% for Unit 6, before modification, are 7400 to 7600 BTU/HP-hr., so the reduction in heat rate is significant.

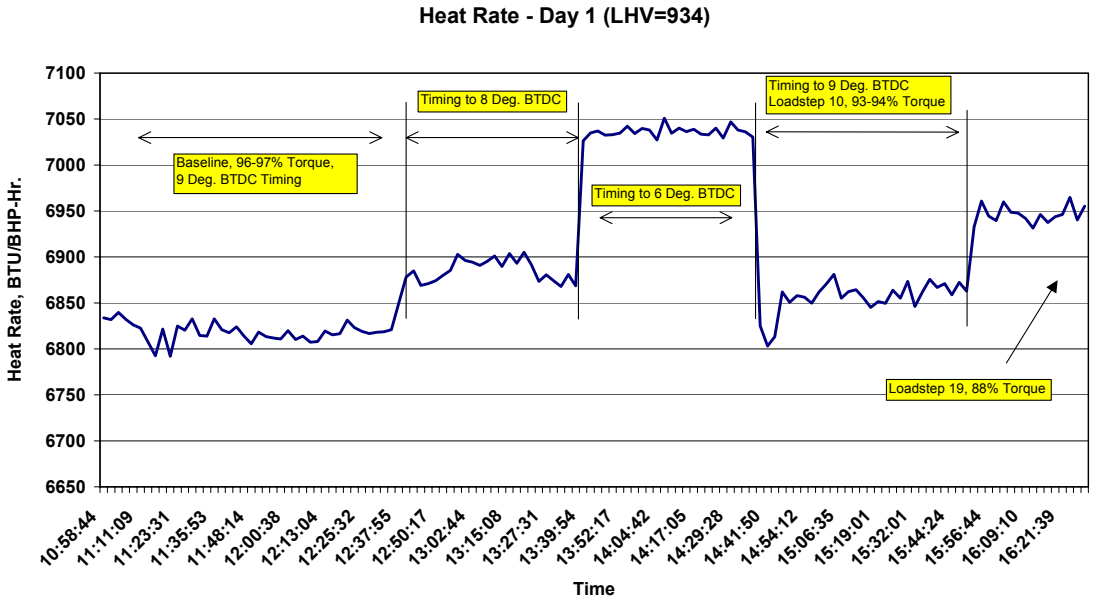

Figure 4-6. Heat Rate; Day 1 Tests; Williams' Station 60; GMW10; Unit 6; After Modifications; August 25, 2004

Figure 4-7 for Day 2 showed the effects of balancing and speed on heat rate. The effects of balancing are very small, though there is some small reduction following CPR balancing. The effect of speed reduction is to increase heat rate, but close examination makes it clear that timing is auto-adjusted when speed is reduced, thus the increases in heat rate can mostly be attributed to the timing retardation - to 4.5 degrees BTDC at 225 RPM.

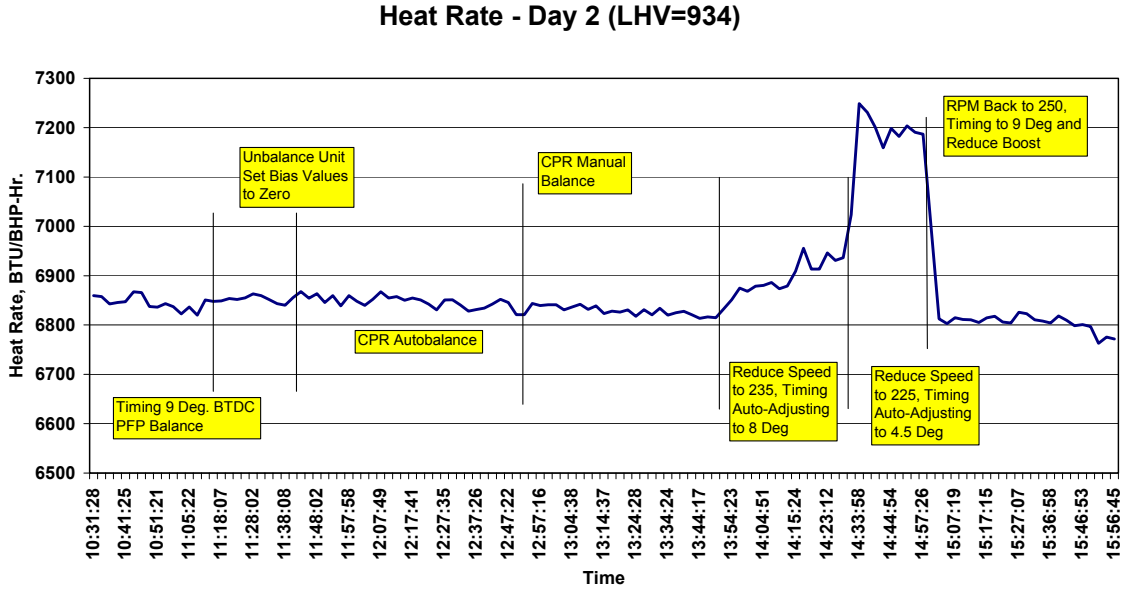

Figure 4-7. Heat Rate; Day 2 Tests; Williams' Station 60; GMW10; Unit 6; After Modifications; August 26, 2004

4.5 COMPRESSOR AND SYSTEM EFFICIENCY

Figures 4-8 and 4-9 present differential indicated power values (DIPs) for the compressor. DIPs are the areas on the compressor cylinders PV card, which lie above the discharge "toe" and below the suction "toe" (the toes are the points of minimum and maximum volume). These DIPs approximate the losses on the basis that the toes approximate line pressures. Thus, a compressor efficiency can be calculated (100% - the DIP percentage for suction and discharge). This basis for efficiency has limitations, but provides a consistent, available method, which has successfully checked against enthalpy rise based methods when tested on earlier project data.

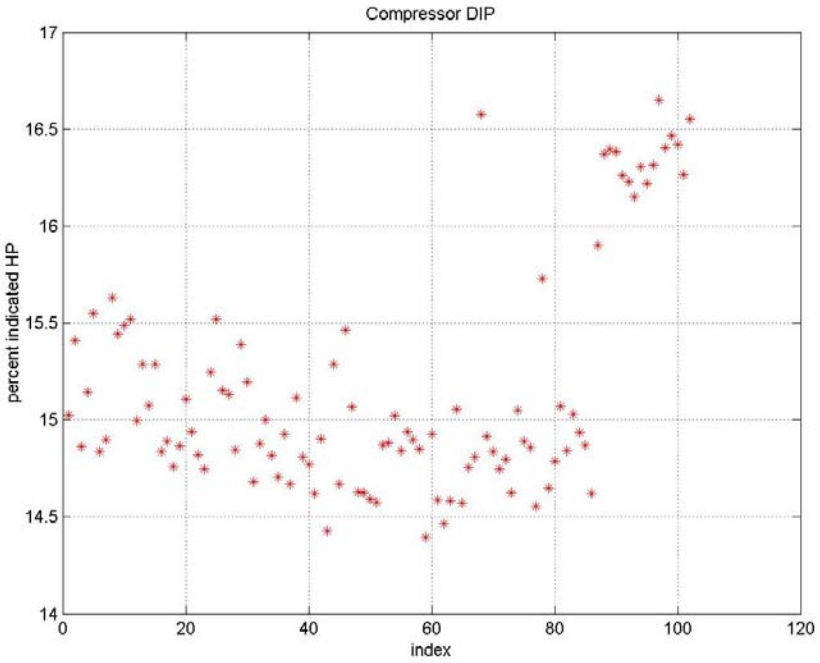

Figure 4-8. Compressor Differential Indicated Power (Sum of Suction and Discharge DIP); Unit 6; After Modification; Day 1; Williams' Station 60; August 25, 2004

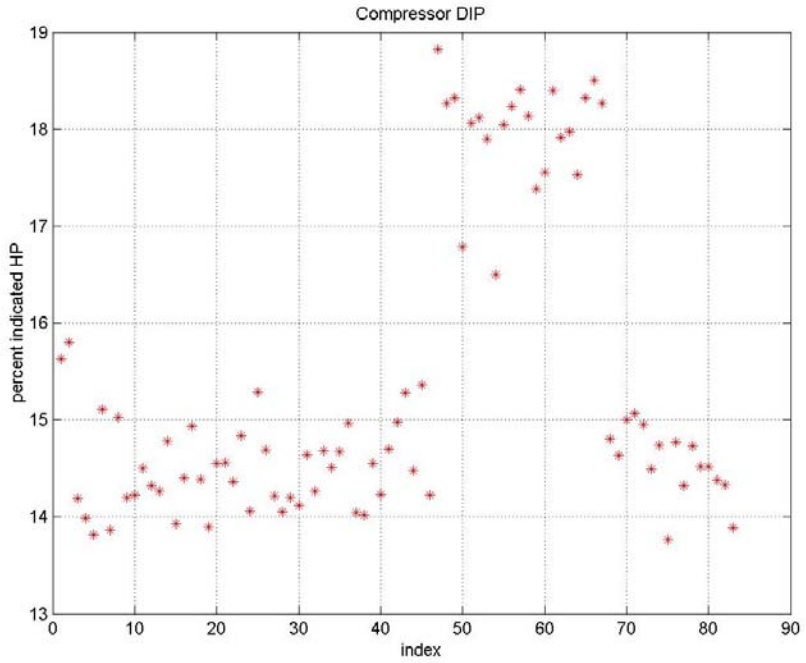

Figure 4-9. Compressor Differential Indicated Power (Sum of Suction and Discharge DIP); Unit 6; After Modification; Day 2; Williams' Station 60; August 26, 2004

Day 1 compressor efficiency (from DIPs) is plotted in Figure 4-10. It starts at about 83.4% and rises very slightly over the first 3.5 hours of testing. The increase in compressor efficiency to about 84.5% between 14:46 and 15:37 appears to correspond directly to the reduction in torque achieved by a change to load step 10. A further reduction in torque to 88% by changing to load step 19 brought the compressor efficiency back close to 83.5%, so it appears to be load step instead of (or in addition to) load which has an influence on compressor efficiency.

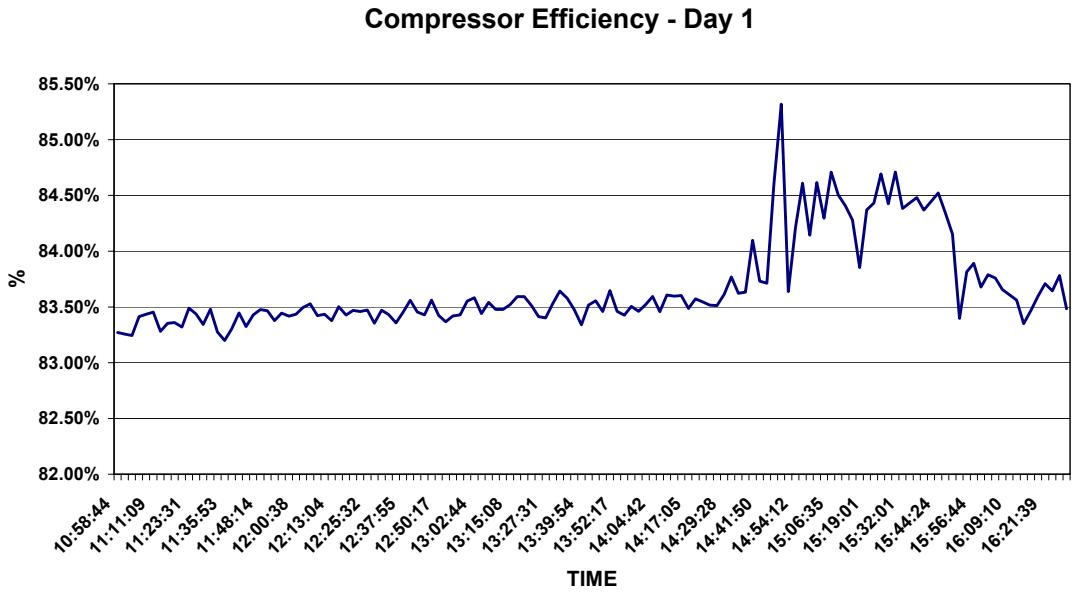

Figure 4-10. Compressor Efficiency from DIP; Unit 6; After Modification; Day 1; Williams' Station 60; August 25, 2004

On Day 2, Figure 4-11 shows the swings in compressor efficiency are more severe and can be directly correlated with speed changes, but not in a monotonic fashion. The biggest drop in compressor efficiency to 75% corresponds to the drop in speed from 250 to 237 RPM. The further drop in speed to 225 RPM appears to result in a small increase to 77.5% compressor efficiency from the low of 75% at 237 RPM.

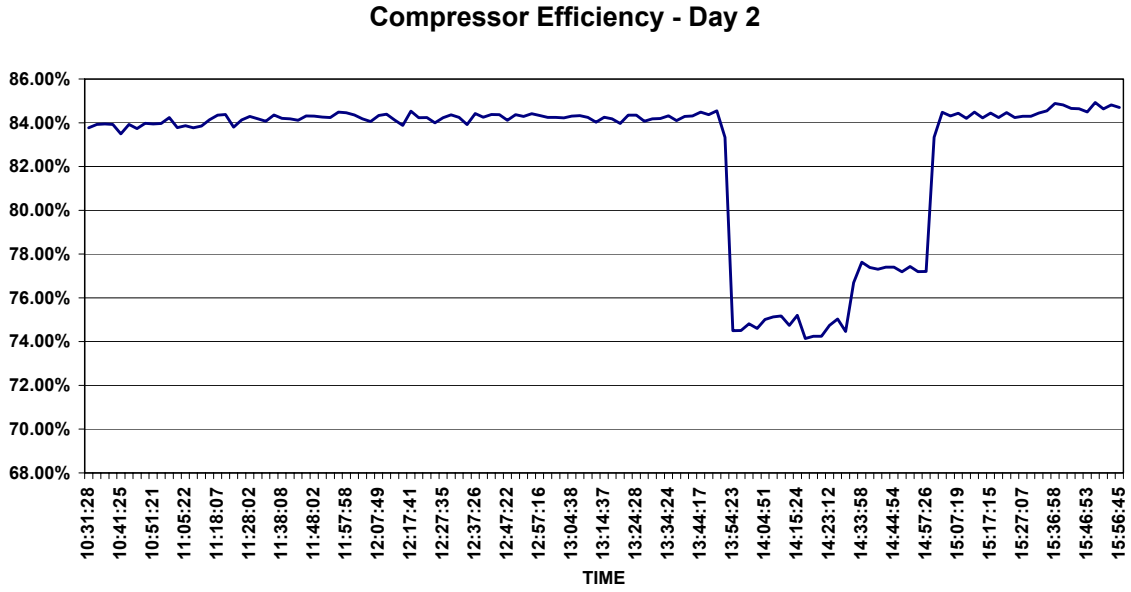

Figure 4-11. Compressor Efficiency from DIP; Unit 6; After Modification; Day 2; Williams' Station 60; August 26, 2004

When the data for compressor efficiency and heat rate are combined with a mechanical efficiency, the result is system thermal efficiency. System thermal efficiency measures the efficiency with which fuel energy is converted to useful compression energy. On Day 1, Figure 4-12 shows that the effects of timing and torque on heat rate are reflected in the system efficiency. The highest efficiency of the day, of about 29.7%, result from a combination of high compressor efficiency at load step 10, combined with 93 to 94% torque, and timing at 9 degrees. The reduction in compressor efficiency combined with the increase in heat rate with torque at 88% reduce overall system efficiency to 29.1% even with 9 degrees BTDC timing.

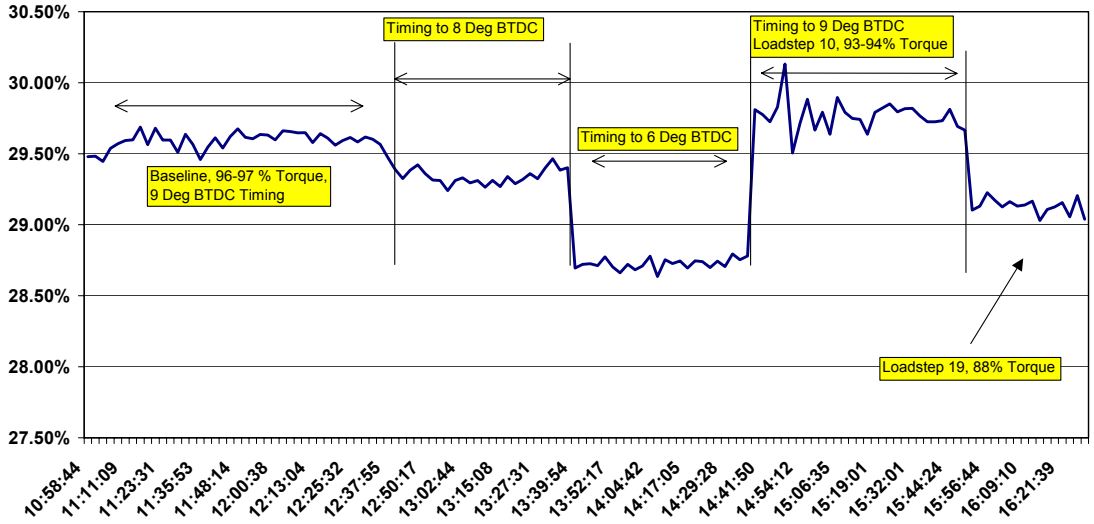

Figure 4-12. Overall System Efficiency; Day 1; (2546.6*Ceff/(HR/0.95); Unit 6; After Modification; Williams' Station 60; August 25, 2004

On Day 2, Figure 4-13 shows overall system efficiency at about 29.8% for much of the day and dropping to 26.3%, and then to 26% with the reductions in speed change to 237 RPM, and then to 225 RPM. These reflect the combination of heat rate increase with auto-retarded timing and the reduction in compressor efficiency with reduced speed. The final condition of Day 2 with speed at 250 RPM, timing at 9 degrees, and boost reduced brings overall system efficiency right up to 30%.

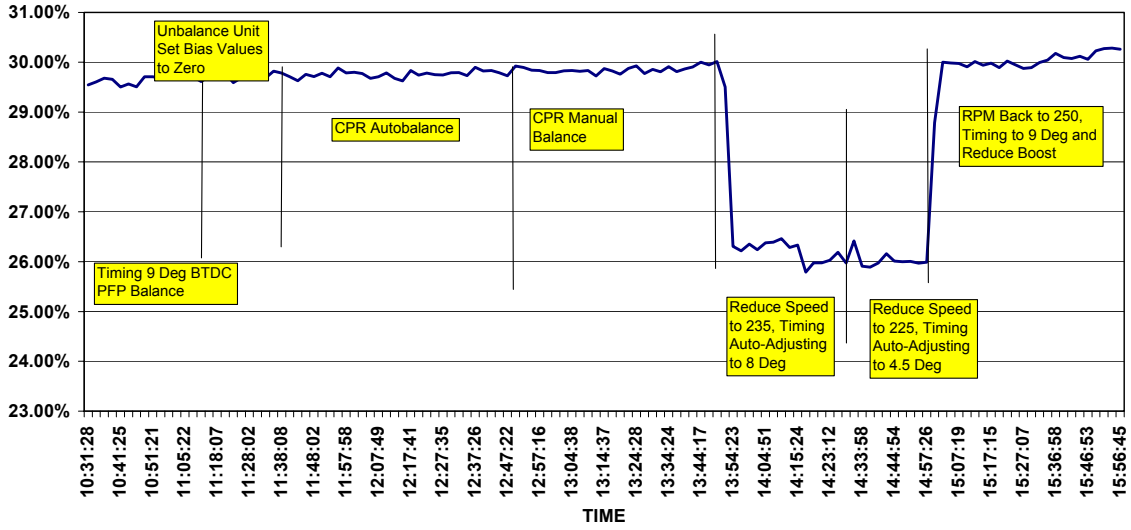

Figure 4-13. Overall System Efficiency; Day 2; (2546.6*Ceff/(HR/0.95); Unit 6; After Modification; Williams' Station 60; August 26, 2004

4.6 CYCLE-TO-CYCLE VARIATION IN PEAK-FIRING PRESSURE

Figure 4-14 shows that the cycle-to-cycle variation in peak-firing pressure for Day 1, quantified as standard deviation, is between 8 and 10% of the average peak-firing pressure. Figure 4-15 shows a similar range on Day 2. The highest values here of 11% correspond to the reduction in speed to 225 RPM. The return to 250 RPM with 9 degrees timing and a reduction in boost cut the standard deviation to below 7%. The richer mixture, which results from reduced boost, could explain this more stable combustion near the end of the day.

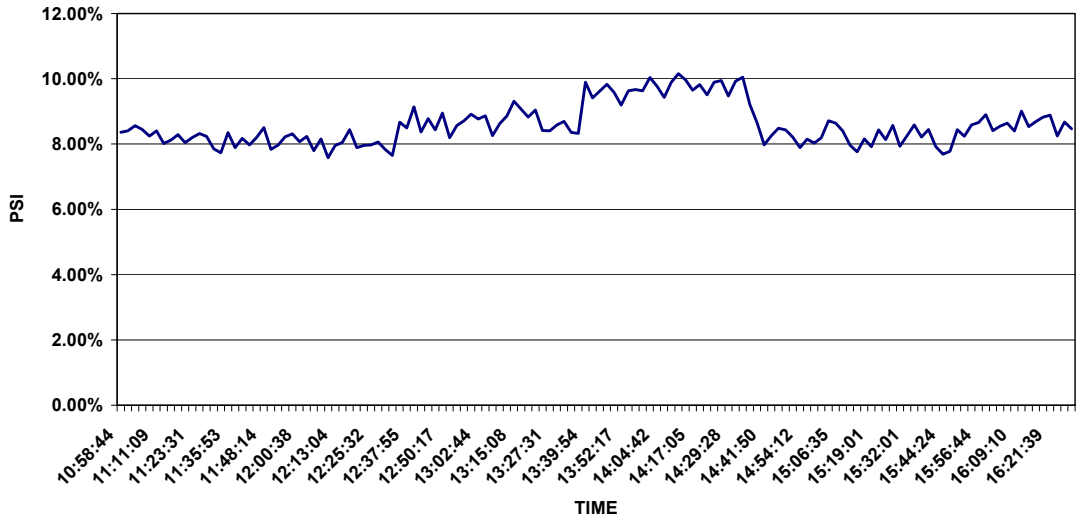

Figure 4-14. Coefficient of Variance (Standard Deviation/Mean) for Peak-Firing Pressure Averaged across the Cylinders; Unit 6; After Modification; Williams' Station 60; Day 1; August 25, 2004

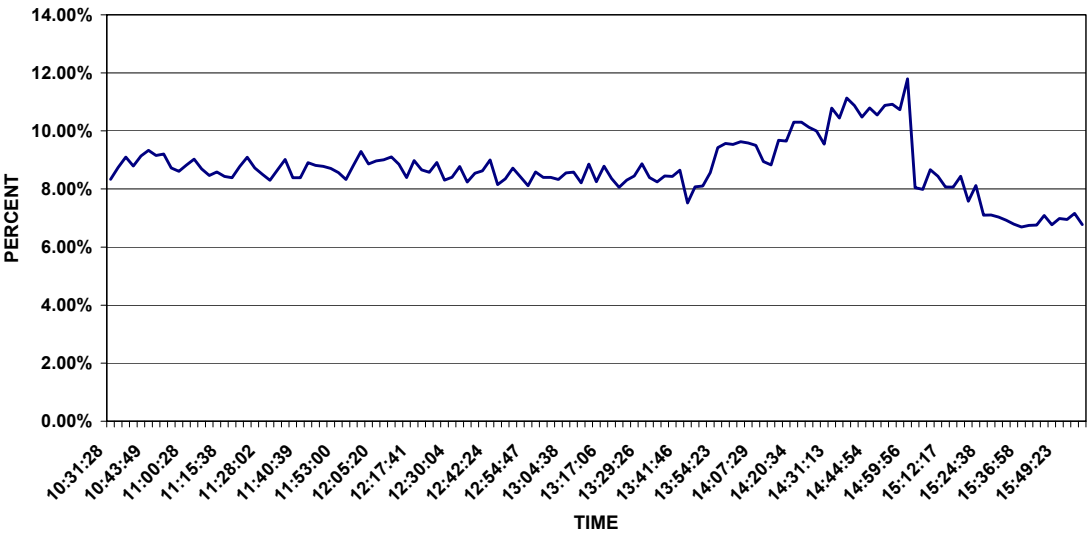

Figure 4-15. Coefficient of Variance (Standard Deviation/Mean) for Peak-Firing Pressure Averaged across the Cylinders; Williams' Station 60; Day 2; August 26, 2004

4.7 CYLINDER-TO-CYLINDER VARIATION AND BALANCING

Figure 4-16 shows the variation in compression pressure with time for each cylinder during the first day and the variation across the cylinders of this compression pressure. The compression pressure is the pressure prior to ignition (we have defined it at 20 degrees before TDC). As with all the other engines tested on this program, there is a spread across the cylinders of compression pressure – in this case about 18 PSI. This spread seems to stay quite constant - even with changes in the average, which approach 20 PSI during the day. On Day 1, the strongest correlation of compression pressure appears to be with load, which was reduced to 93%, and then to 88% at the end of day1.

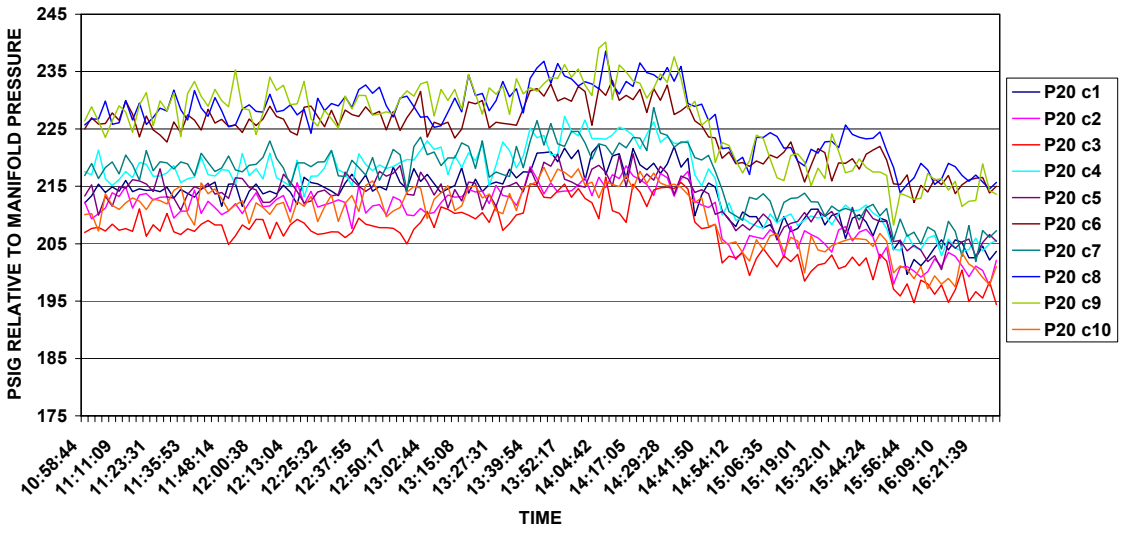

Figure 4-16. Compression Pressure; Williams' Station 60; Unit 6; After Modification; Day 1; August 25, 2004

Figure 4-17 shows the same spread in compression pressure on Day 2, and less change in the average compression pressure. The reduction in boost at the end of Day 2 has the strongest influence on average compression pressure, causing about 10 PSI reduction.

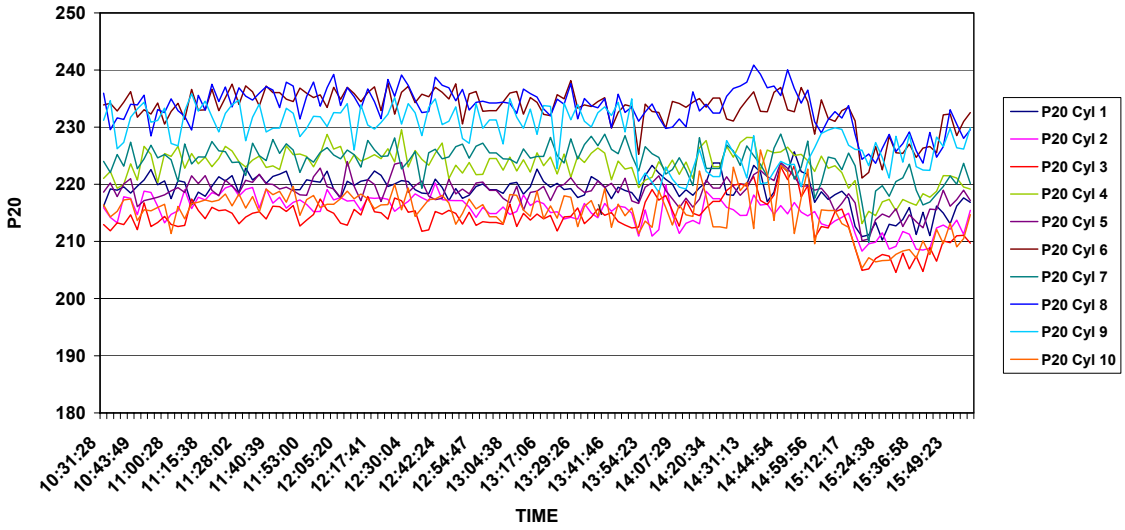

Figure 4-17. Compression Pressure; Day 2; Unit 6; After Modification; Williams' Station 60; August 26, 2004

Figure 4-18 shows the Day 1 variation of spread in peak-firing pressure, and in combustion pressure ratio (CPR). The level varies early in the day, ranging up to 18% for CPR, and to 15% for peak-firing pressure. During this early increase, the timing was in its "as found" condition of 9 degrees and the torque was at 96 to 97%. During the subsequent changes in timing and load (after 12:30), the spreads remained fairly constant at 5% for CPR and 10% for PFP, except for a sharp transient around 15:00 when timing and load step were changed.

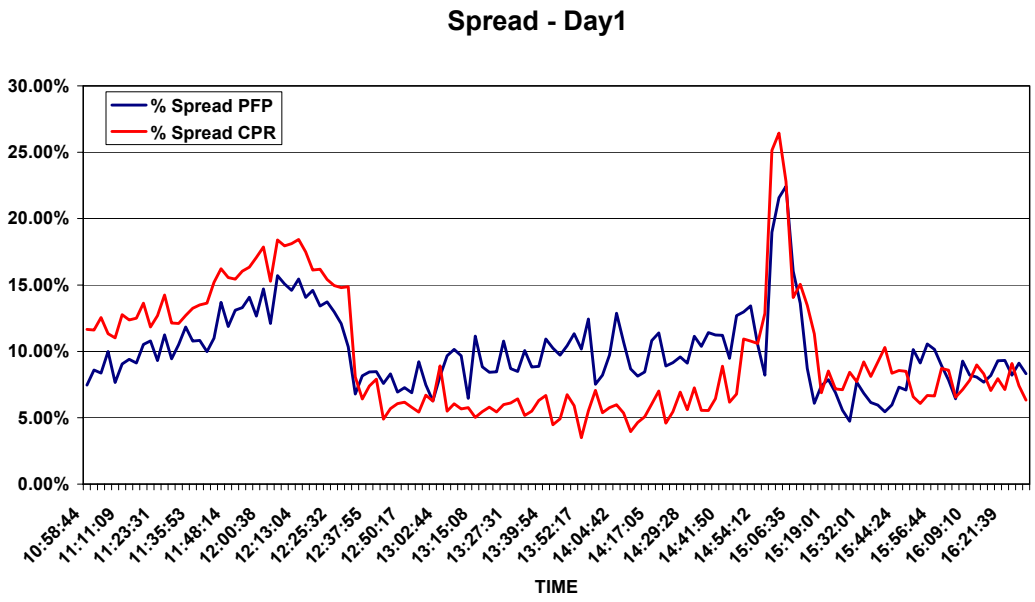

Figure 4-18. Percentage Spread for Time-Averaged Peak-Firing Pressure; Unit 6; After Modification; Williams' Station 60; Day 1; August 25, 2004

Figure 4-19 shows the spread on the second days testing when balancing tests were performed. From 10:30 to 11:15, manual balancing on peak-firing pressure was performed and reduced the spread in both PFP and CPR (but most strongly in PFP to 5% as would be expected). After this, the fuel valves were opened to unbalance the unit and automatic CPR balancing was started. The automated algorithm had been installed by Enginuity, and clearly started to move cylinder fuel steadily in the right direction to reduce spread in PFP and CPR. However, the controls were set to make only slow changes and after an hour, CPR spread had dropped only from 30% to 25%. At this point, manual CPR balancing was initiated and rapidly reduced CPR spread to 5%, leaving PFP spread at about 12%. Between 13:54 and 15:07, speed change tests were performed with the fuel valves left as at the end of manual CPR balancing. The speed changes clearly caused the spread in both CPR and PFP to increase.

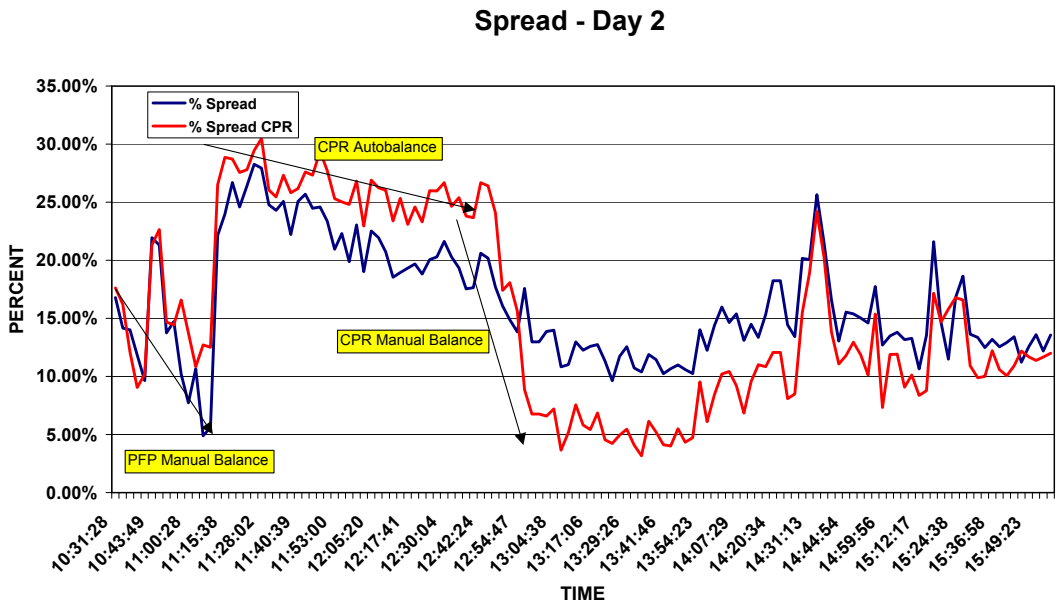

Figure 4-19. Percentage Spread for Time-Averaged Peak-Firing Pressure; Unit 6; After Modification; Williams' Station 60; Day 2; August 26, 2004

Figure 4-20 shows the instantaneous spread in peak-firing pressure for Day 1, and Figure 4-21 shows it for Day 2. The instantaneous spread represents the difference between highest and lowest in a single cycle (revolution), and this instantaneous spread is averaged over a number of cycles. It is clear that in any revolution, the variation in peak-firing pressure is around 30% to 35% of the mean value, and that balancing to reduce the spread in average pressure has only a small influence on the instantaneous spread - reducing it at best to a little below 30%. As a specific example, manual balancing of peak-firing pressure early in Day 2 reduces the spread in average peak pressure by a factor of 3, while the instantaneous spread only drops from 30% to 28%. This is a rationale for why balancing of any sort has only a small influence on heat rate, as previously discussed with respect to Figure 4-7.

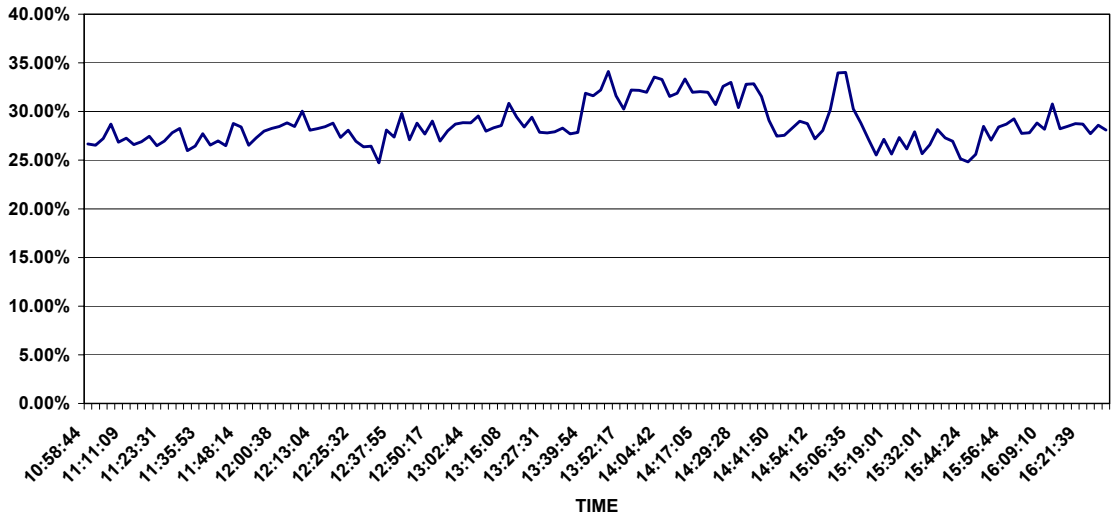

Figure 4-20. Instantaneous Spread Averaged over Multiple Cycles; Day 1; Unit 6; After Modification; Williams' Station 60; August 25, 2004

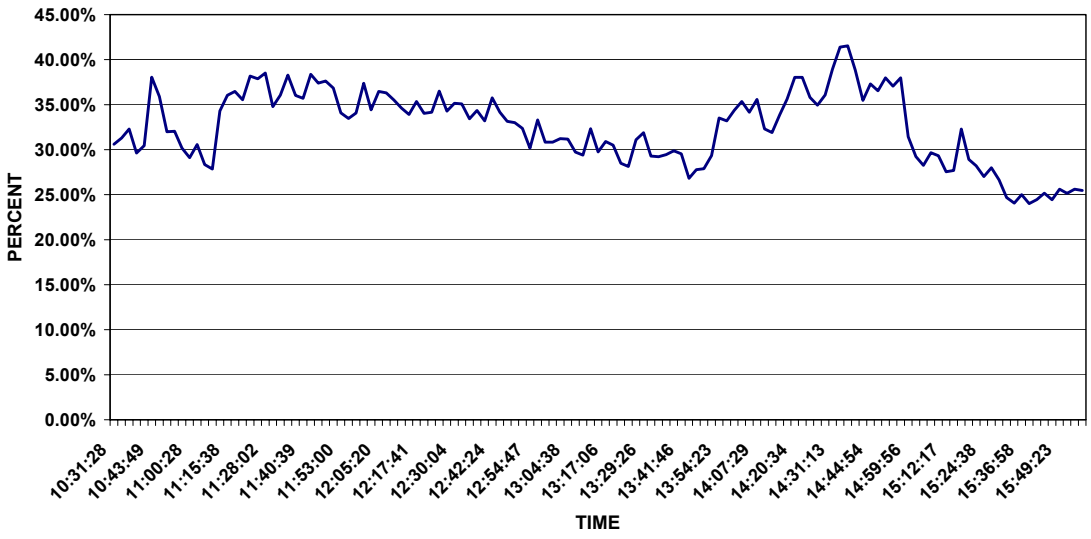

Figure 4-21. Instantaneous Spread Averaged over Multiple Cycles; Day 2; Unit 6; After Modification; Williams' Station 60; August 26, 2004

4.8 GLOBAL EQUIVALENCE RATIO AND EMISSIONS

Figures 4-22 and 4-23 show the global equivalence ratio and normalized NOx concentration on days 1 and 2. The timing and load changes on Day 1 clearly influence the NOx concentration – retarding timing from 9 to 6 degrees BTDC reduces NOx – about by a factor of 2 from between 0.21 and 0.25 to 0.11. The influence of load is less definitive, but there is some indication that reducing load reduces NOx. The global equivalence ratio is in the range 0.43 to 0.45 on Day 1.

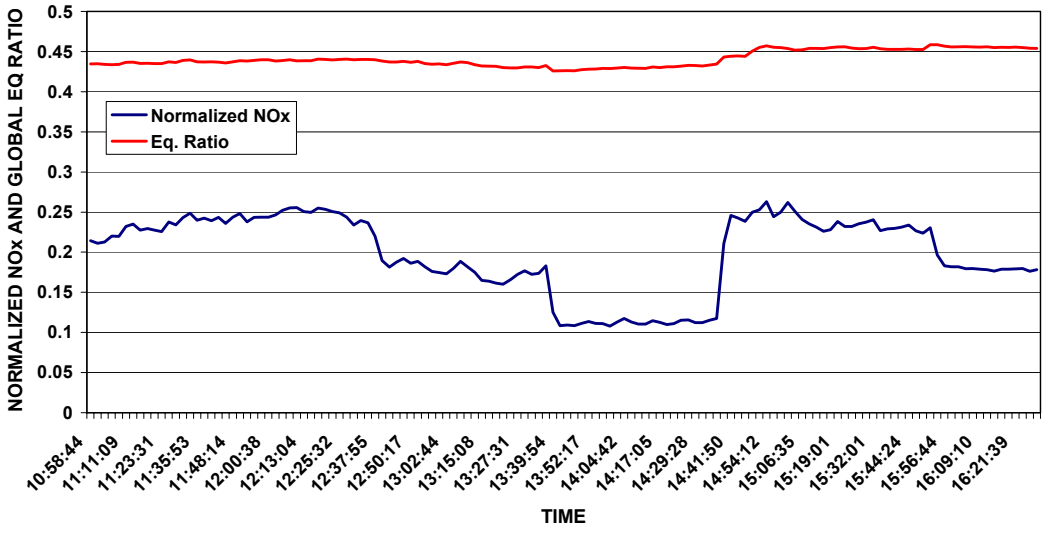

Figure 4-22. Normalized NOx Concentration and Global Equivalence Ratio; Unit 6; After Modification; Williams' Station 60; Day 1; August 25, 2004

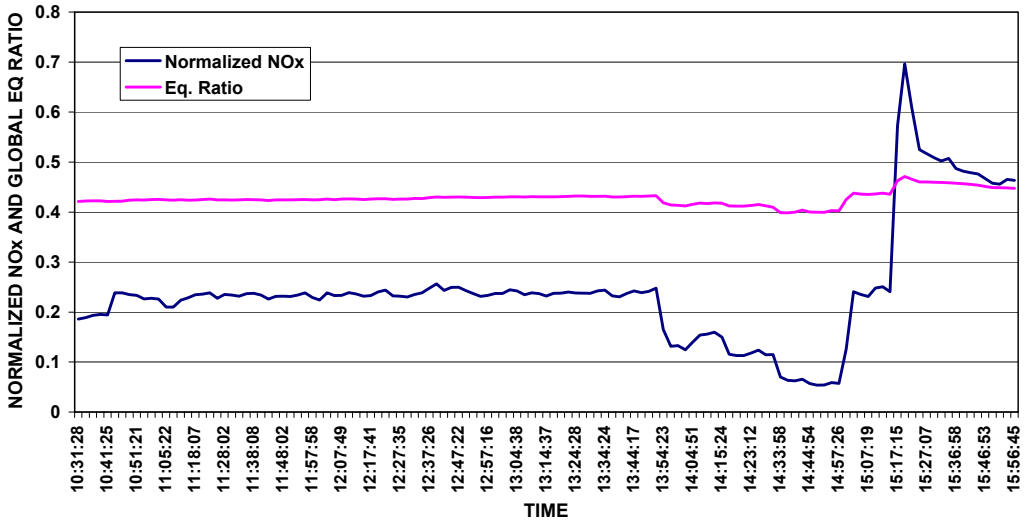

Figure 4-23. Normalized NOx Concentration and Global Equivalence Ratio; Unit 6; After Modification; Williams' Station 60; Day 2; August 26, 2004

On Day 2, the NOx concentration stays rather constant for most of the day at 0.22, in spite of balancing changes. Reducing speed reduces NOx substantially, by a factor of 3 for the reduction in speed from 250 to 225. After speed was returned to 250, the NOx seems to return momentarily to its previous level of about 0.23. It then jumps monetarily to 0.7 – probably a transient result as boost was reduced, since it then starts to drop, reaching about 0.47, and then stays at this level - probably reflecting the steady influence of a richer mixture. Global equivalence ratio stays at 0.43 most of the day, then drops with speed reduction and returns to 0.43 at 250 RPM. The further increase in equivalence ratio to 0.45, as boost was dropped, is apparent.

4.9 PEAK-FIRING PRESSURE

Figures 4-24 and 4-25 show the variation of peak-firing pressure averaged over all cylinders. On Day 1, it starts at 560 PSI and drops with retarded timing to 488 PSI at 6 degrees BTDC, and returns to 560 PSI when timing is returned to 9 degrees BTDC. The reduction in torque to 88% near the end of the day drops the PFP to 530 PSI. It is to be noted that prior to the modifications, the averaged peak-firing pressure at about 102% torque and 6° timing was 600 PSI; for 8° timing, it was 700 PSIG. These numbers compare to 488 and 560 PSIG at 96 to 97% torque for the modified unit, indicating a significant reduction after modification, even when the torque difference is considered.

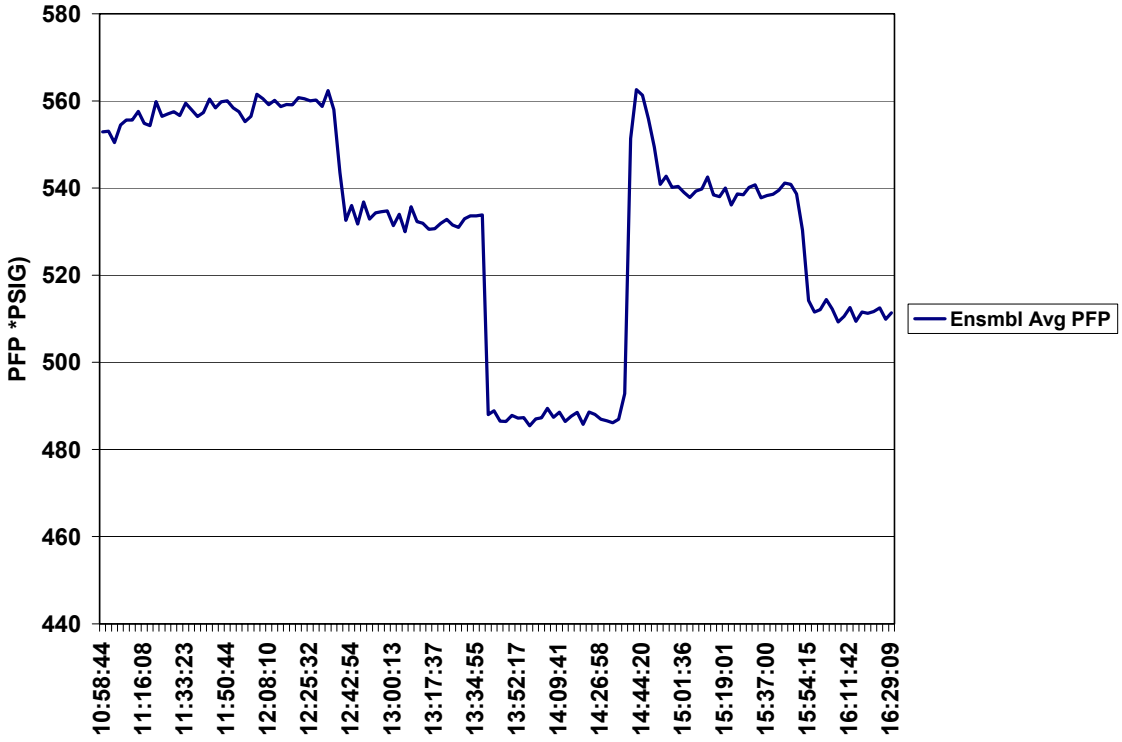

Figure 4-24. Average Peak-Firing Pressure for All Cylinders; Unit 6; After Modification; Williams' Station 60; Day 1; August 25, 2004

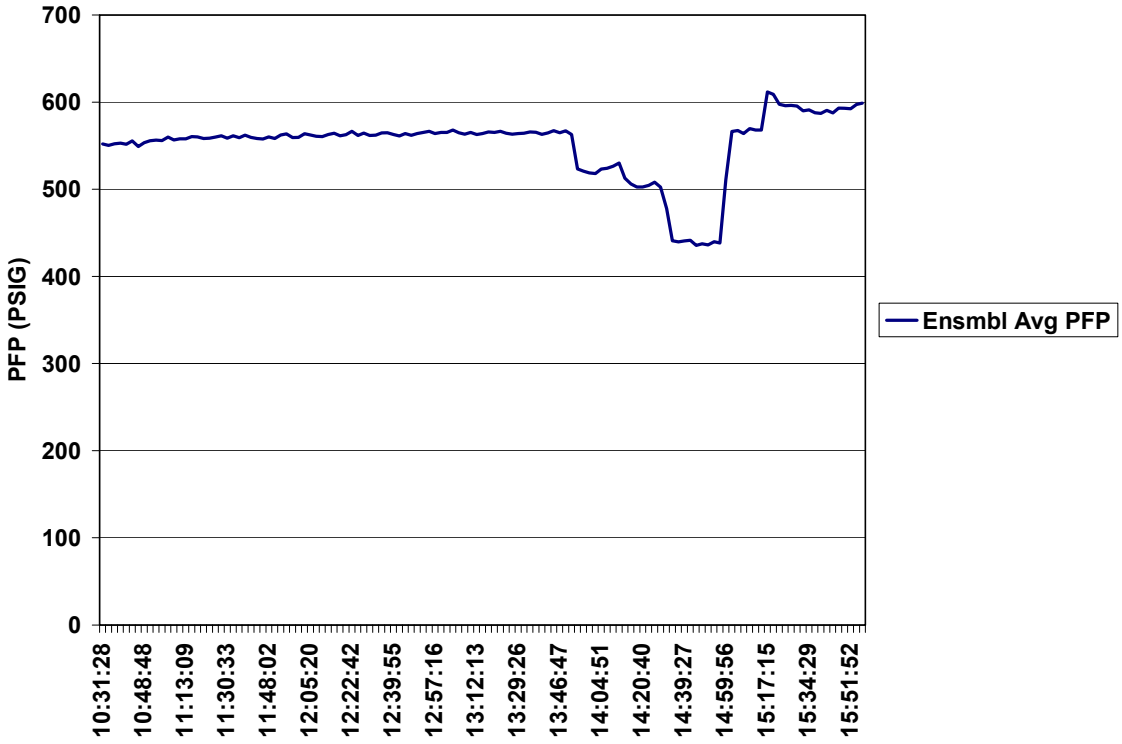

Figure 4-25. Average Peak-Firing Pressure for All Cylinders; Unit 6; After Modification; Williams' Station 60; Day 2; August 26, 2004

On Day 2, the PFP stays around 550 during the balancing tests - then drops noticeably with speed reduction - probably strongly influenced by the auto-retard of timing. It returns for a short period to just over 550 - then undergoes some transients as boost is reduced.

4.10 ROD LOAD MONITOR (RLM) TESTING

Figures 4-26 and 4-27 compare power from the rod load monitor against power determined from the dynamic pressures of the two cylinder ends. The numbers clearly track directly and any changes in load are reflected in both sources of data for both days. There is an offset between the two sources of 5 to 10 HP, and a small difference, such as this is not surprising. Figures 4-28 and 4-29 present this difference as a percentage, which ranges from 0.9% to 1.6% on Day 1 and between 0.9 and 2.7% on Day 2. The biggest percentage discrepancy occurs when speed is dropped. It should be recognized that there are various potential sources of discrepancy between these two sources of power values. Firstly, the RLM depends on assumed material properties

and rod dimensions. Secondly, the RLM measurement is made upstream of the cylinder pressure in the power flow chain and piston ring/rider band losses would cause a difference. Third, although the pressure transducers are calibrated, there exists some residual error in the pressure values. Thus, a 1 to 3% discrepancy between these two sources is not surprising; at the same time, the uncertainty will need to be minimized in application of the RLM. The commercializing partner for the RLM has suggested the use of a static pressure calibration using deadweighted pressure to the cylinder. Alternatively, since cylinder indicated power using calibrated pressure transducers is the standard at present, a calibration based on indicated power is an option. Whatever method is used, the friction losses in the rings and rider bands need to be recognized in application of RLM power.

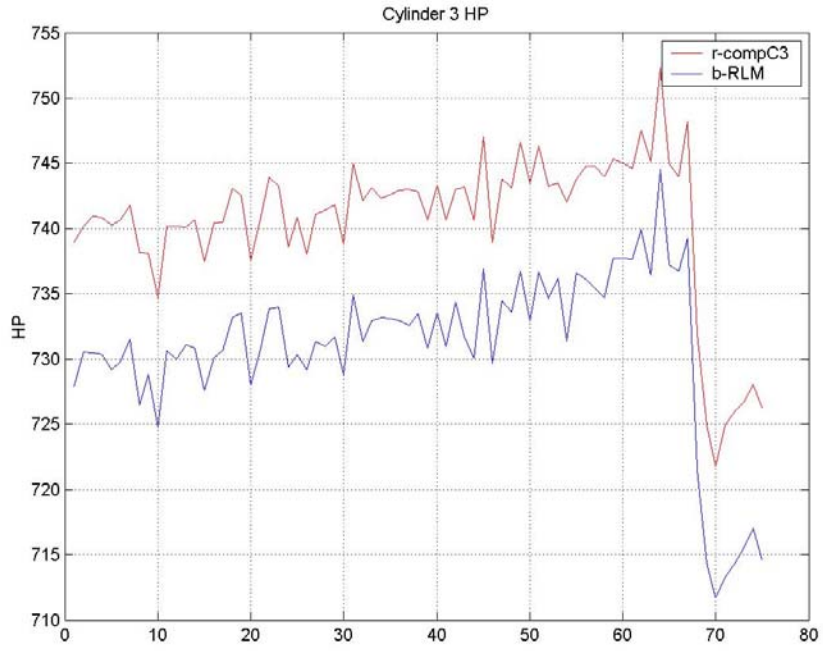

Figure 4-26. Comparison of Horsepower based on the Rod Load Monitor and on Cylinder Pressure; Unit 6; After Modification; Williams' Station 60; Day 1; August 25, 2004

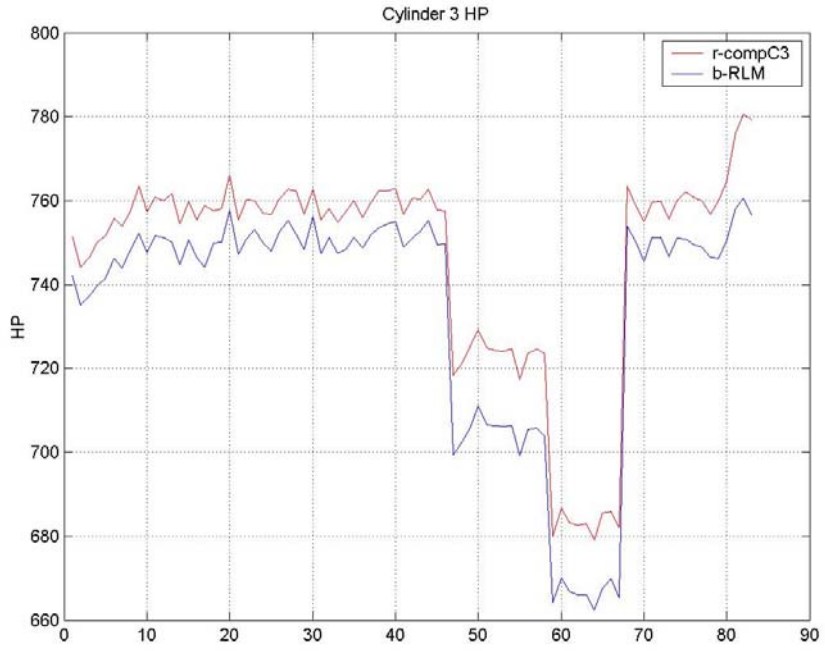

Figure 4-27. Comparison of Horsepower based on the Rod Load Monitor and on Cylinder Pressure; Unit 6; After Modification; Williams' Station 60; Day 2; August 26, 2004

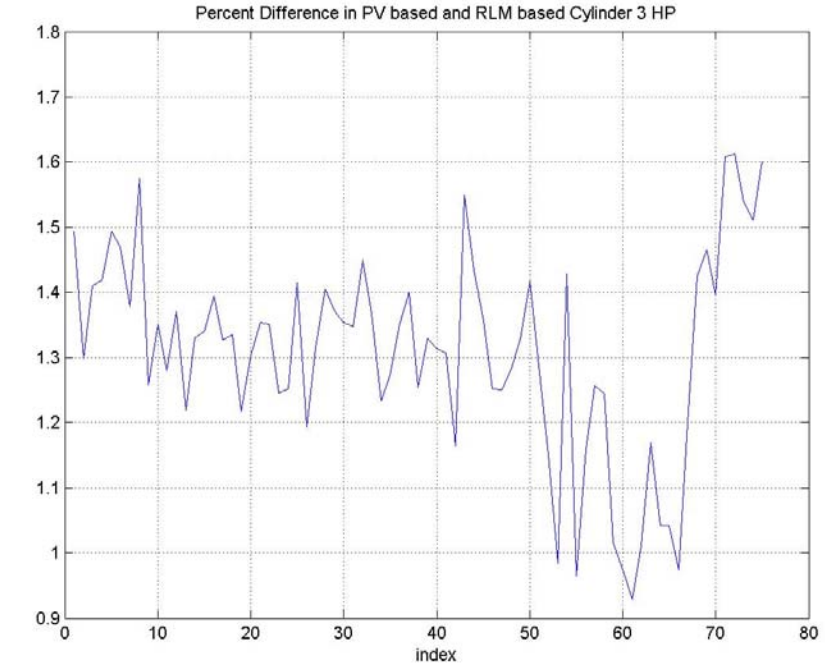

Figure 4-28. Percentage Difference between Horsepower based on Rod Load Monitor and on Cylinder Pressure; Unit 6; After Modification; Williams' Station 60; Day 1; August 25, 2004

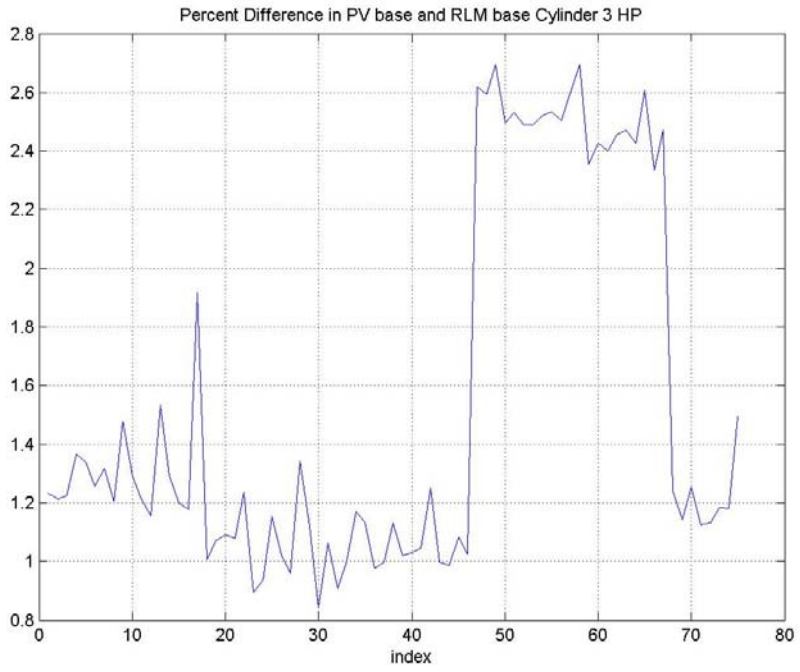

Figure 4-29. Percentage Difference between Horsepower based on Rod Load Monitor and on Cylinder Pressure; Unit 6; After Modification; Williams' Station 60; Day 2; August 26, 2004

4.11 AIR MANIFOLD PRESSURE

Figures 4-30 and 4-31 present the variation in manifold dynamic pressure range at the measurement point, expressed as a percentage of the average manifold pressure. The dynamic range of between 21% and 29% on Day 1 and between 16% and 27% on Day 2 is typical of previous observations for MAP. The values drop below 22% on Day 2 when the speed is reduced, suggesting that there could be a change in acoustic response in the air manifold as a function of speed. It is noteworthy that the compression pressure spread from Figure 4-17 does appear to exhibit small change in characteristics and range when the speed changes between 13:44 and 14:57.

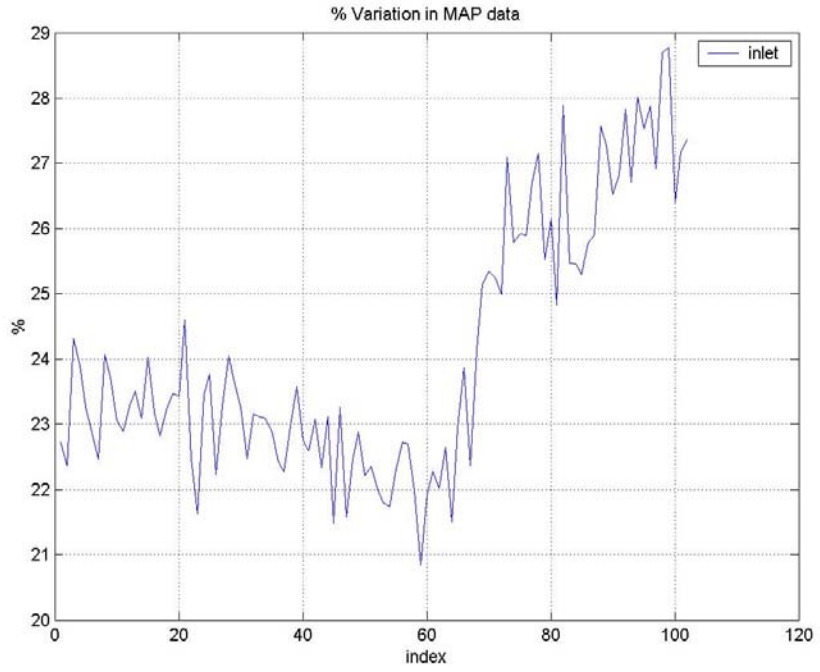

Figure 4-30. Normalized Percentage Range of Air Manifold Pressure Variation over a Revolution (Range/Average %); Unit 6; After Modification; Williams' Station 60; Day 1; August 25, 2004

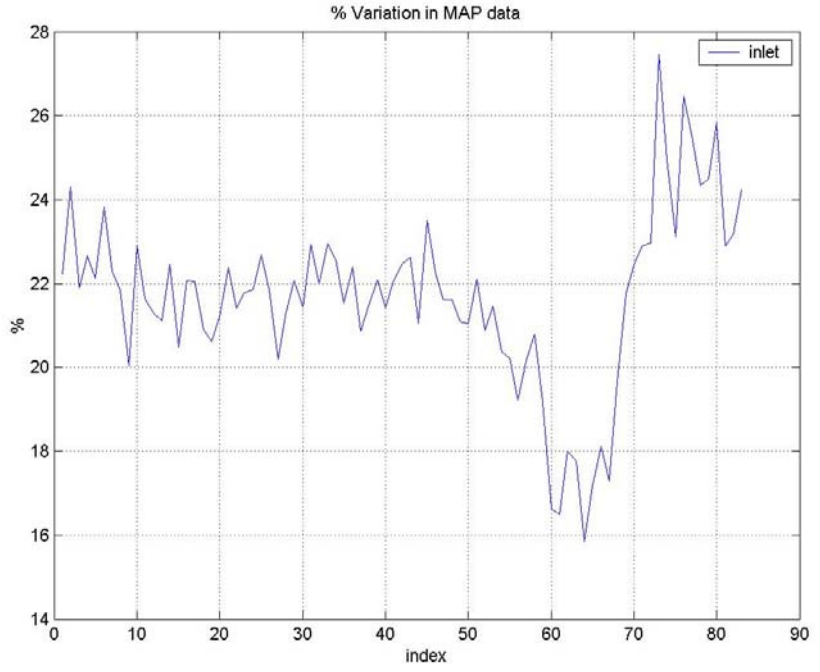

Figure 4-31. Normalized Percentage Range of Air Manifold Pressure Variation over a Revolution (Range/Average, %); Unit 6; After Modification; Williams' Station 60; Day 2; August 26, 2004

4.12 TORSIONAL VIBRATION

Figure 4-32 shows how the crankshaft instantaneous velocity varies during Day 2. It stays in the range 3 to 5.5% for the first 55 records (index), then starts to increase as speed is cut from 237 to 225 RPM. This may indicate the reduced speed approaches closer to a torsional resonance.

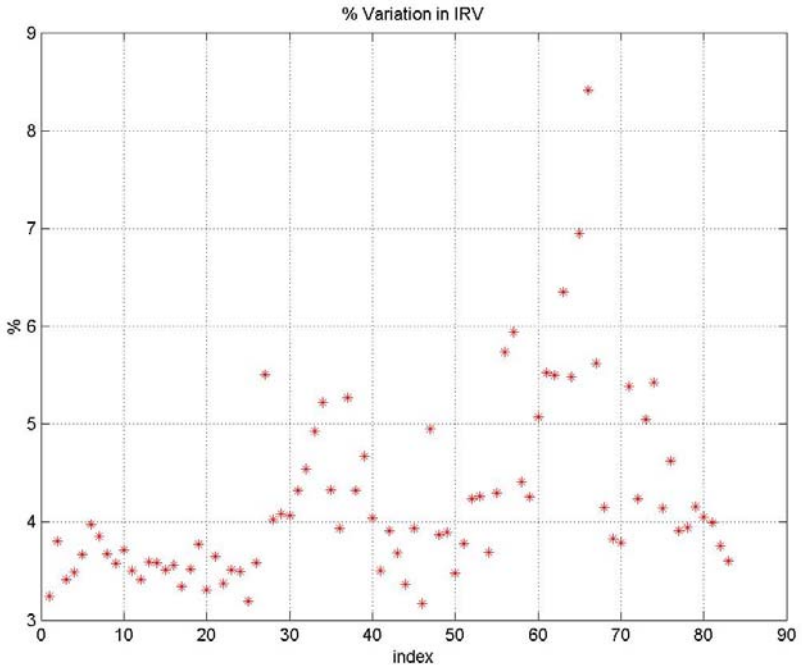

Figure 4-32. Normalized Percentage Variation in Instantaneous Rotational Velocity (Range/Average, %); Unit 6; After Modification; Williams' Station 60; Day 2; August 26, 2004

4.13 CRANKSHAFT STRAIN

Figures 4-33 and 4-34 present waveforms of crankshaft strain over eight revolutions measured on Day 1 and Day 2, respectively. These waveforms are similar to those obtained on other units, with strong first and second order components.

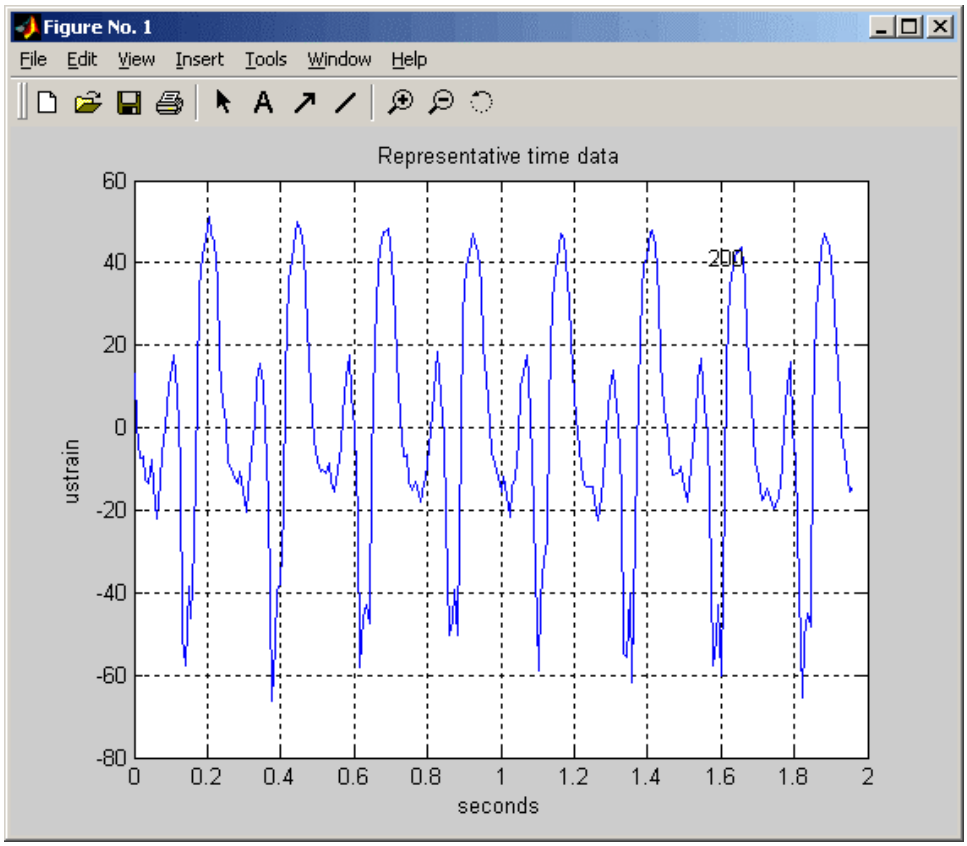

Figure 4-33. Waveform over Eight Revolutions for Crankshaft Strain Monitor Output; Unit 6; After Modification; Williams' Station 60; Day 1; August 25, 2004

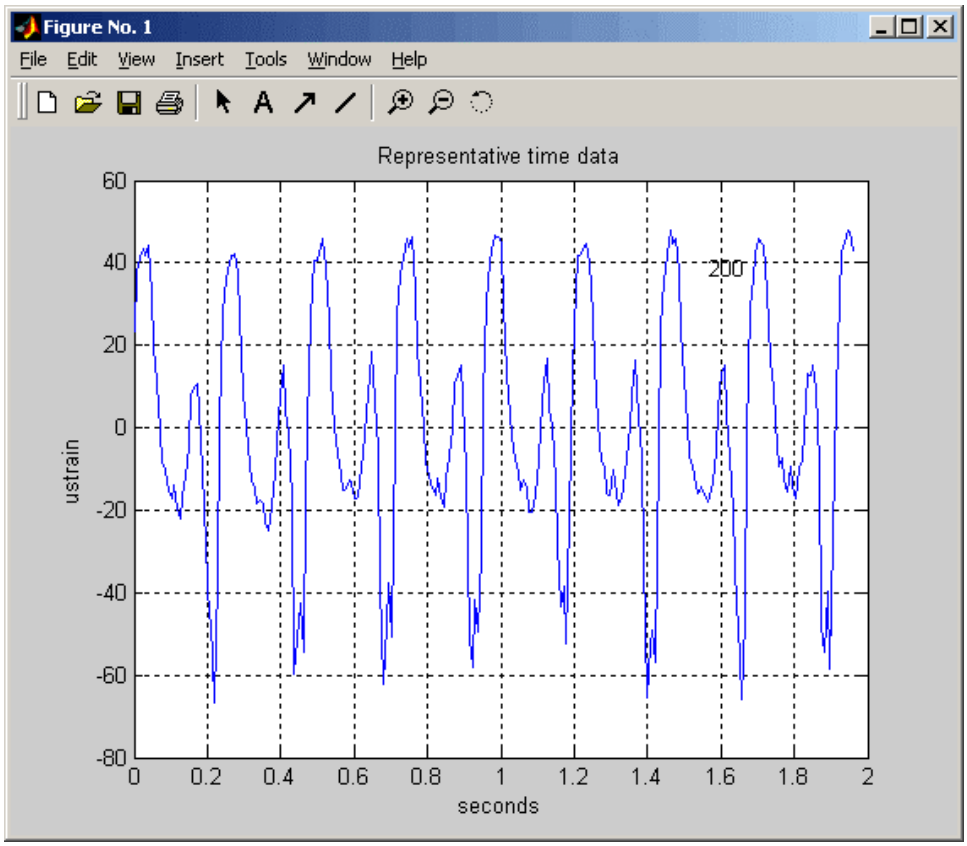

Figure 4-34. Waveform over Eight Revolutions for Crankshaft Strain Monitor Output; Unit 6; After Modification; Williams' Station 60; Day 2; August 26, 2004

Figures 4-35 and 4-36 present the variation of peak-to-peak crankshaft strain with test time for the two days. On Day 1, up to 100 minutes, this data should be discounted because efforts were underway to eliminate detonation. After this, the Day 1 strain is at about 115 microstrains for about 2.5 hours. At about 270 minutes, timing is retarded to 8 degrees BTDC and at 330 minutes, it is further retarded to 6 degrees BTDC. The trend downwards in crankshaft strain over this period is apparent, with crankshaft strain falling to below 110 microstrains. Close to 400 minutes, timing is returned to 9 degrees and the strain goes up, but load step is then changed to bring the torque down to 93%, and the strain drops to below 110 microstrains again. A further reduction to 88% at about 460 minutes reduces the microstrain down to about 103.

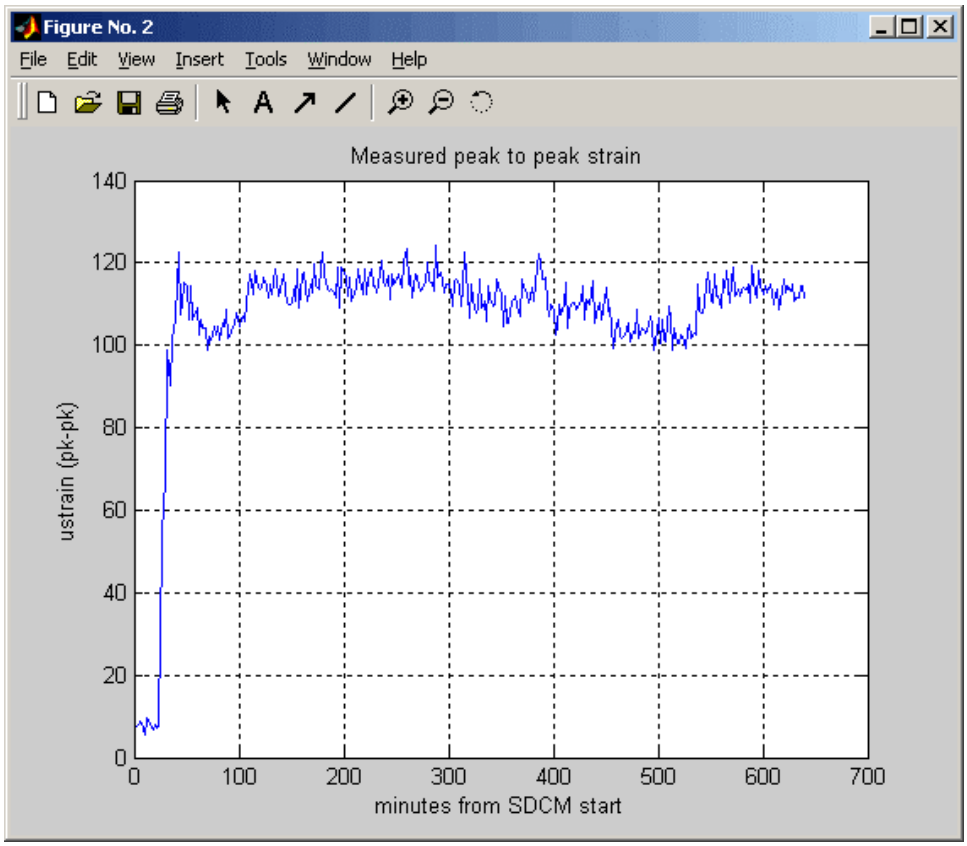

Figure 4-35. Peak-to-Peak Dynamic Variation in Crankshaft Microstrain; Unit 6; After Modification; Williams' Station 60; Day 1; August 25, 2004

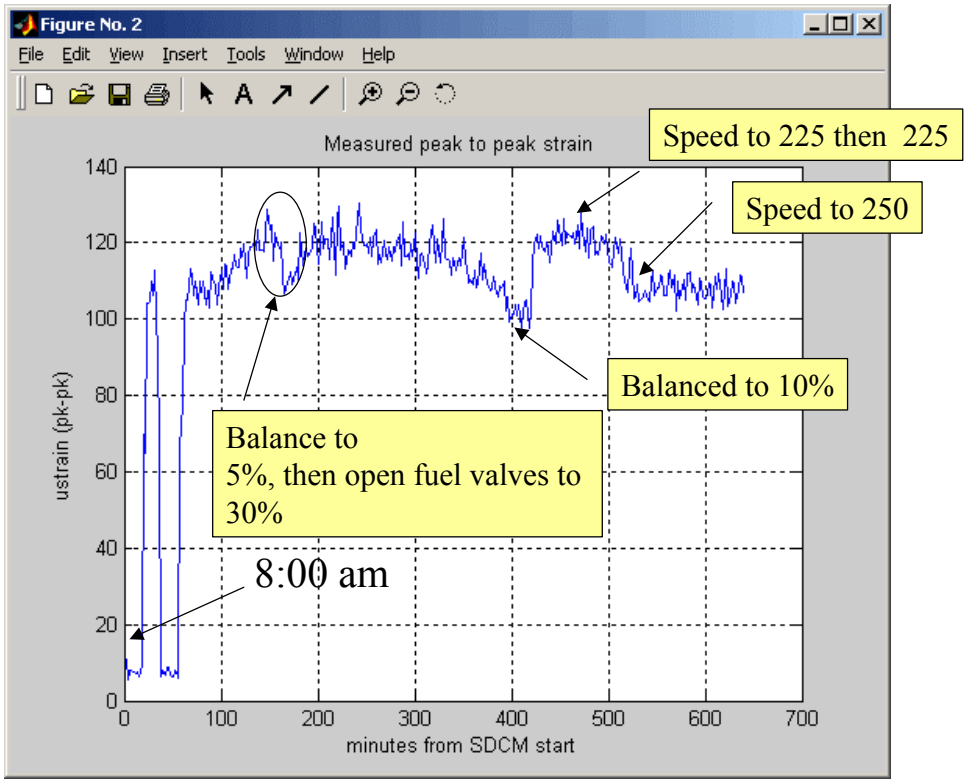

Figure 4-36. Peak-to-Peak Dynamic Variation in Crankshaft Microstrain; Unit 6; After Modification; Williams' Station 60; Day 2; August 26, 2004

It is noted that the tests on the same unit before modification for high-pressure fuel showed close to 120 microstrains for 6 degrees BTDC timing, and then 130 to 140 microstrains for 8 degrees BTDC timing. The data discussed above for the modified unit shows 110 microstrains at 6 degrees, and 115 microstrains at 8 degrees. Thus, there is apparently about 10% reduction in strain following the modification, although part of this difference is attributable to lower torque and Day 1 of the tests presented here.

On Day 2, the peak-to-peak microstrain appears to respond to balancing, and to speed changes. At around 150 to 200 minutes, the unit was first manually balanced to 5% on PFP. This correlates directly with a reduction in strain from 120 to 108 microstrains. The fuel valves were then opened and the microstrain went up to 120 – then followed first the automatic balancing, which appears to produce a slight, but slow reduction in strain. At about 350 minutes, the faster manual CPR balancing was initiated and the microstrain dropped to 100 as the CPR spread was reduced to 5%, and the PFP spread was reduced to 10%.

The subsequent cut in speed to 237 and then to 225 RPM increased the strain to 120, which is likely a result of the closer proximity to a torsional resonance as observed in the IRV data when speed was cut. Increasing the speed back to 250 RPM cut the microstrain back to about 107.

Figures 4-37 and 4-38 present the dynamic orders of the crankshaft strain signal as a waterfall plot, with dominance in the first two orders.

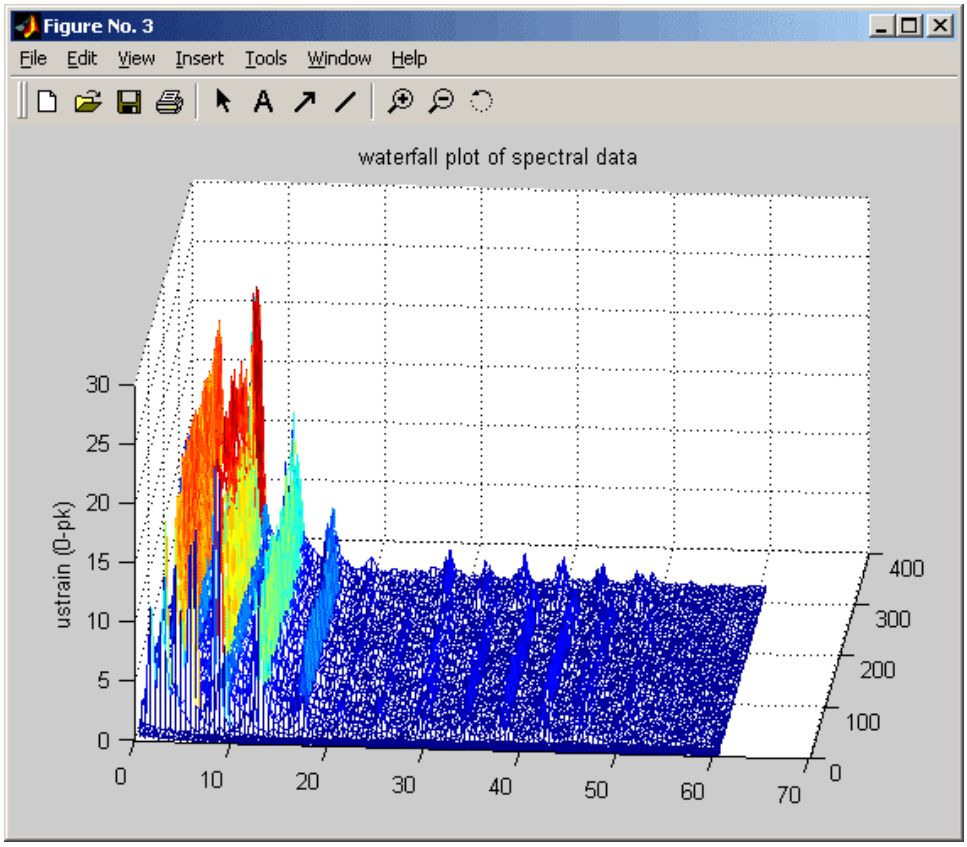

Figure 4-37. Waterfall Plot of Crankshaft Dynamic Microstrain Variation (Zero-to-Peak); Unit 6; After Modification; Williams' Station 60; Day 1; August 25, 2004

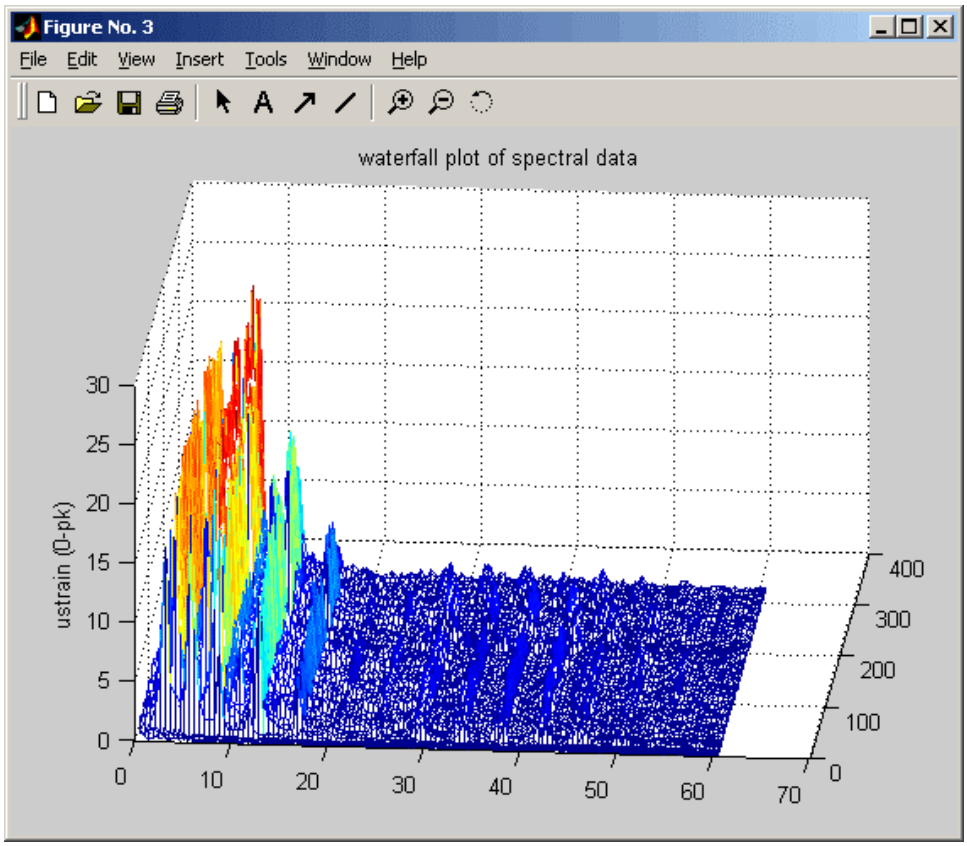

Figure 4-38. Waterfall Plot of Crankshaft Dynamic Microstrain Variation (Zero-to-Peak); Unit 6; After Modification; Williams' Station 60; Day 2; August 26, 2004

Figures 4-39 and 4-40 present the same data with the first eight orders as a function of time. These figures, again, emphasize the dominance of the first two orders, which track each other quite closely on the first day. The third order is about half the level of the first two and the fourth order is down by a factor of 2 again. It appears that in the higher orders, the seventh and eighth order exceeds the fifth and sixth orders.

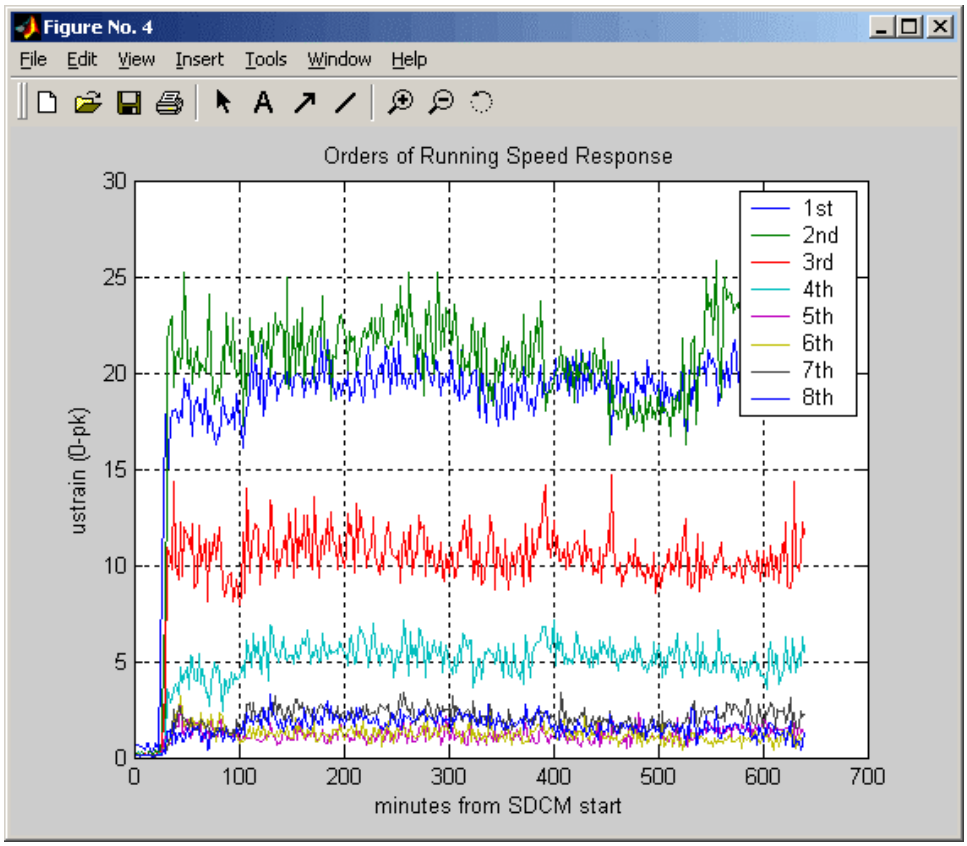

Figure 4-39. Spectral Orders of Crankshaft Dynamic Microstrain Variation; Unit 6; After Modification; Williams' Station 60; Day 1; August 25, 2004

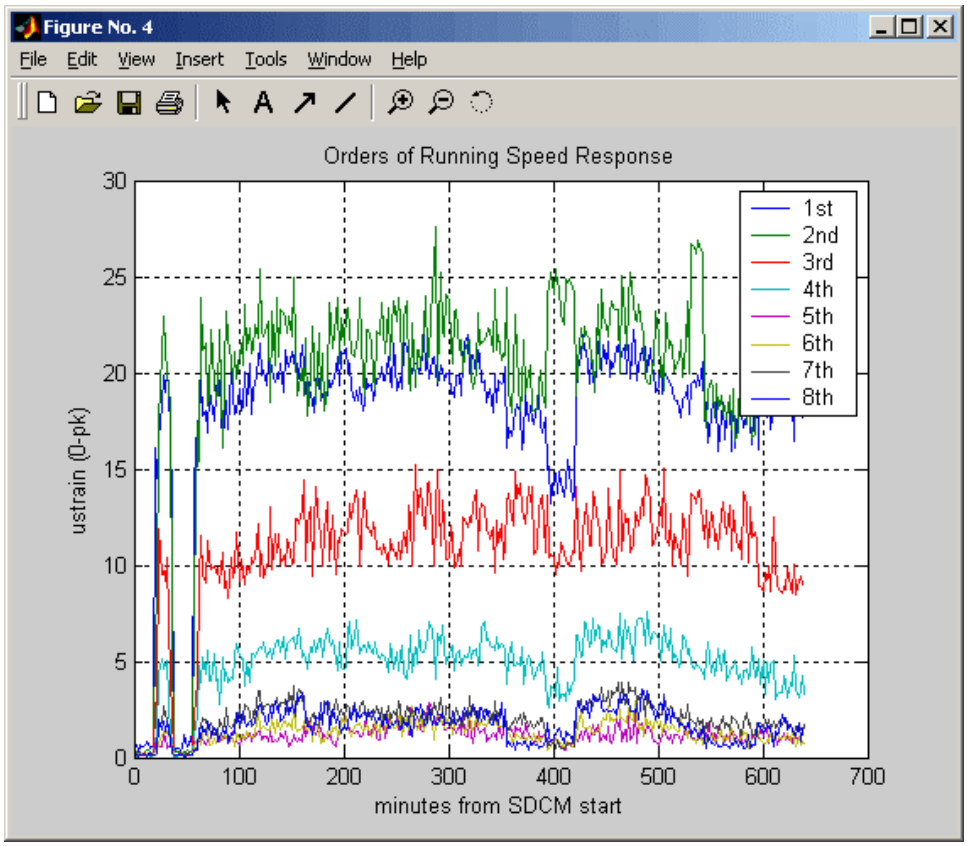

Figure 4-40. Spectral Orders of Crankshaft Dynamic Microstrain Variation; Unit 6; After Modification; Williams' Station 60; Day 2; August 26, 2004

The changes in strain with timing and torque appear to show most strongly in the first two orders in Day 1. On Day 2, the reduction in first and second orders with PFP balancing may be seen at 160 minutes, and the effect of CPR balancing is particularly strong on the first order at around 400 minutes.

4.14 DETECTION OF DETONATION

Figures 4-41 and 4-42 present a comparison of peak power cylinder pressure and detonation detector output for Day 1 on Cylinder 4 (left). This device was loaned to the project by Metrix. The data starts between 8:30 and 9:00 when the unit was started and found to be detonating. Fuel adjustments were made and the detonation was corrected after about 30 minutes. The knock sensor was clearly at 4 to 5 volts much of the time in the first hour, and the peak-firing pressure reached as high as 700 PSI; the detonation was audible. The peak pressure is actually

an average, so the highest excursions associated with detonation were undoubtedly higher than 700 PSI. After this cylinder was stabilized, its peak pressure was reduced to about 550 PSI, and the knock detector's output dropped to below 1.5 volts for the rest of the day.

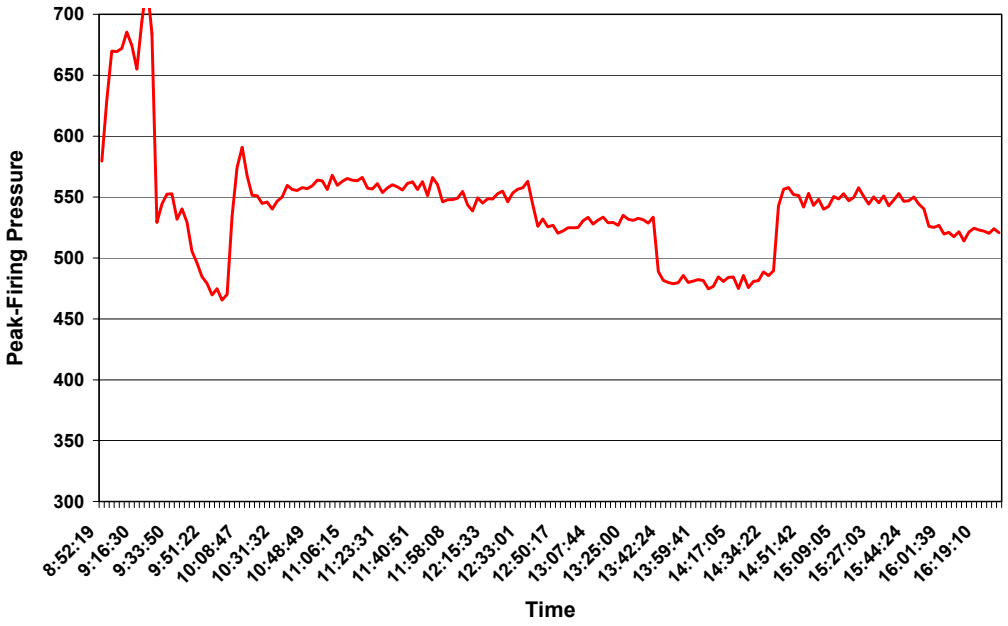

Figure 4-41. Power Cylinder 4 (Left); Average Peak-Firing Pressure; Unit 6; After Modification; Williams' Station 60; Day 1; August 25, 2004

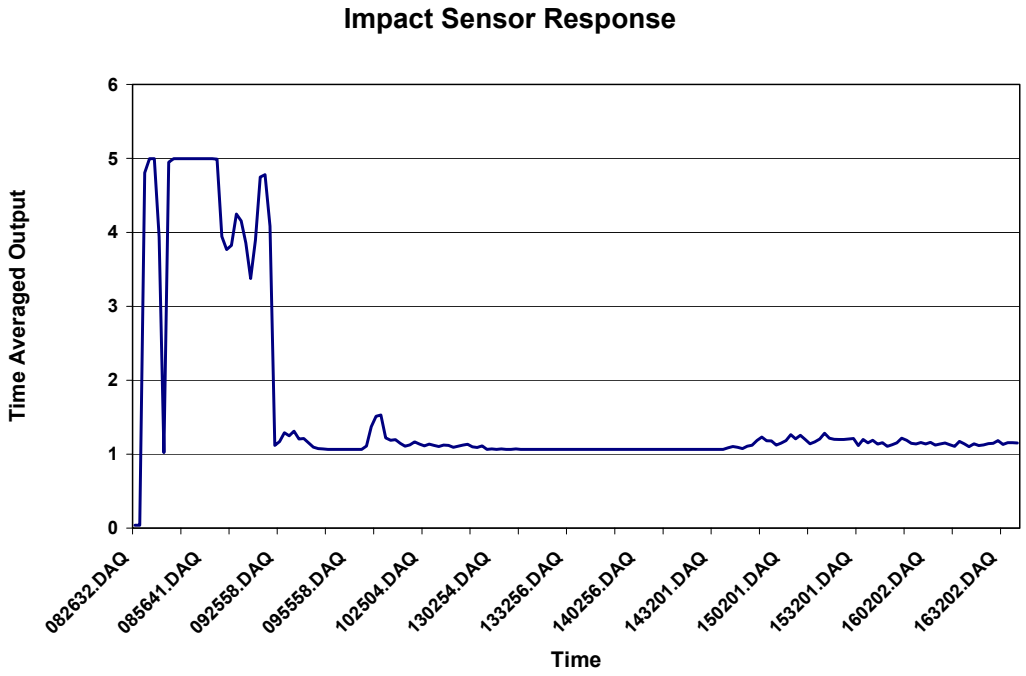

Figure 4-42. Detonation Detector Signal Corresponding to Figure 4-41; Unit 6; After Modification

Figures 4-43 and 4-44 show the same comparison of Cylinder 4L peak-firing pressure and the knock detector output on Day 2. The peak pressure shows a momentary spike for a few minutes around 9:40, and the knock detector jumped to almost 2 volts. There was no audible detonation at this time. Towards the end of the day, the peak pressure jumped to over 675 PSI, and the knock detector output jumped to almost 4 volts. The detonation was again audible, and probably the actual peak pressure excursions were higher than 675 PSI.

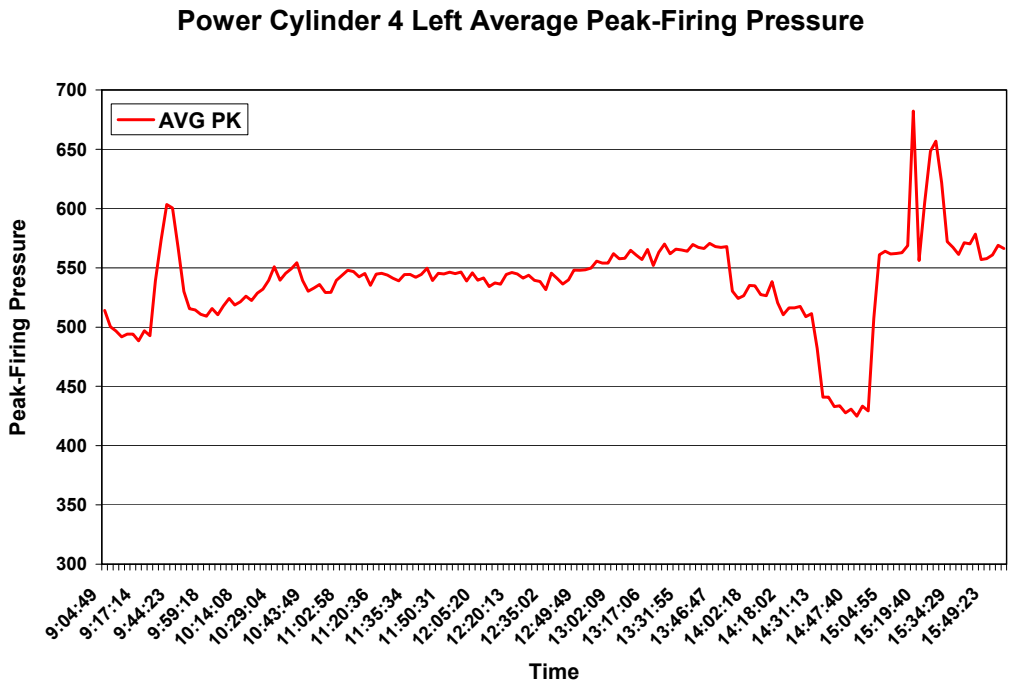

Figure 4-43. Power Cylinder 4 (Left); Average Peak-Firing Pressure; Unit 6; After Modification; Williams' Station 60; Day 2; August 26, 2004

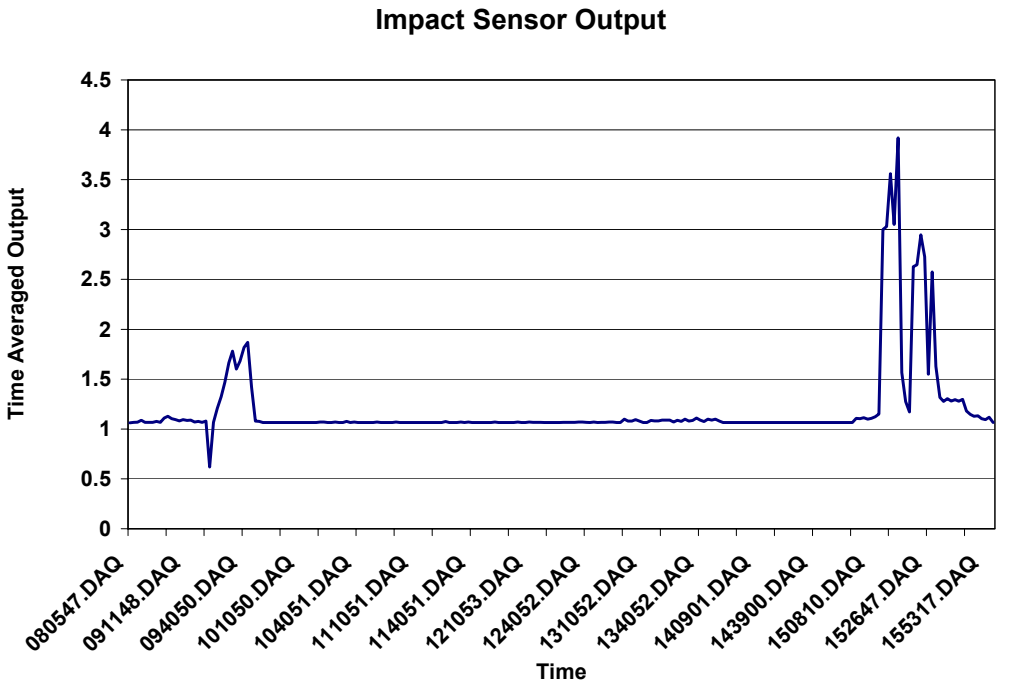

Figure 4-44. Detonation Detector Signal Corresponding to Figure 4-43; Unit 6; After Modification

Based on these results, the value of this detonation detector was demonstrated. Whenever audible detonation occurred, the output voltage exceeded 4 volts. Thus, taking corrective action against detonation at a threshold in the range of 2.5 or 3 volts would appear to provide safe protection against damaging detonation. This is closely consistent with previous tests.

4.15 INFLUENCE OF TORQUE AND TIMING

During both days testing, the engine torque was generally below 100%. Figures 4-45 and 4-46 document this based on data logged, with Williams assistance, from their station data system. During the first day's testing, there was an overt effort made to change the torque and changes to load step 10, and then to 19 achieved reduction in torque, however, it was believed that the 96% to 97% level was as high as could be achieved under prevailing pipeline conditions. Review of data from August, when the unmodified unit was tested, show that the torque was then in the 101% to 102% range. Thus, some further analysis and data re-normalization will be required to align the data sets to a common torque and provide the most meaningful quantitative comparison.

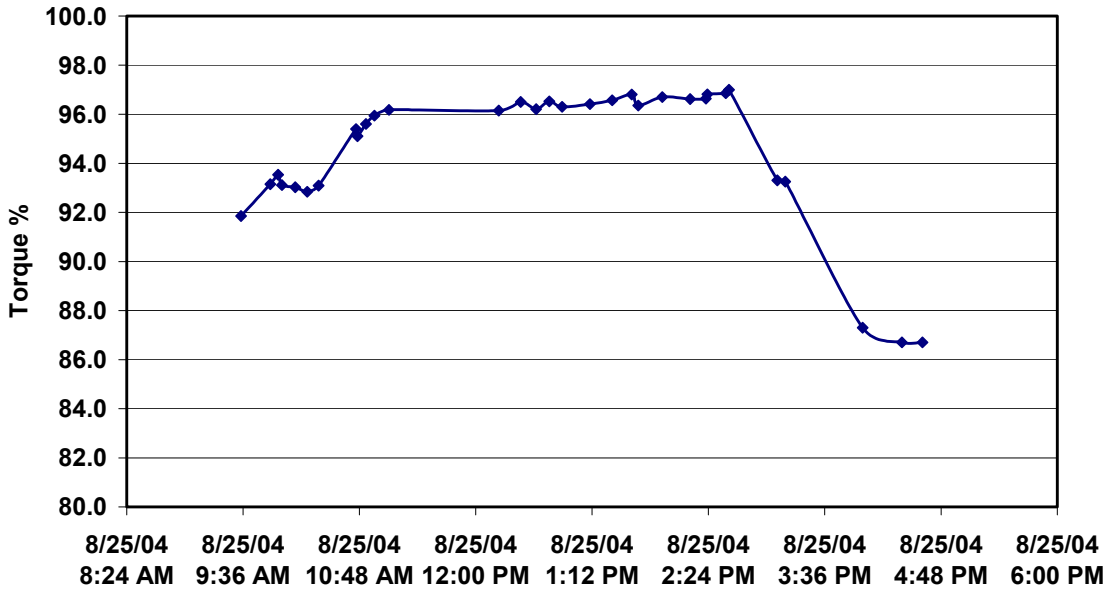

Figure 4-45. Percentage Torque on Day 1; Unit 6; After Modification; Williams' Station 60; August 25, 2004

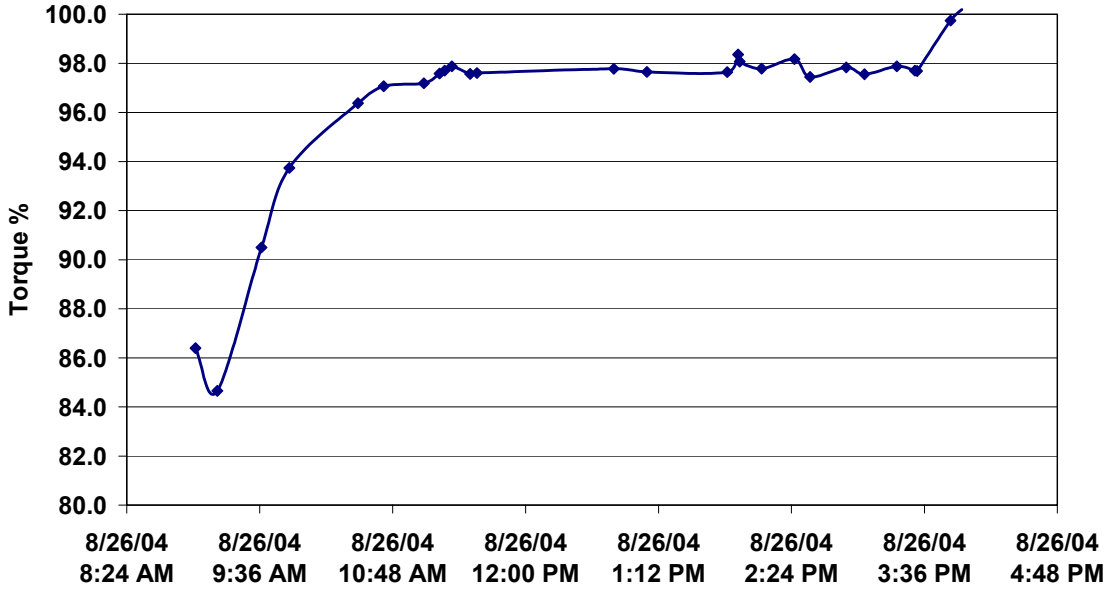

Figure 4-46. Percentage Torque on Day 2; Unit 6; After Modification; Williams' Station 60; August 26, 2004

This comparison is also complicated by timing considerations. The timing range covered in February was 6° and 8° before top dead center (BTDC), with the "nominal" or "as found" value at 6°. The timing range covered in the August tests was 6°, 8°, and 9° BTDC, with 9° as the "nominal" or "as found" condition. Comparisons need to be made at comparable torques and timing values, and it will require some further re-normalization to align both torque and timing. Thus, while the benefits in heat rate, NOx reduction, and crank strain reduction are clear, the conclusions will remain quantitative until this comparative analysis is complete.

As a start on this analysis and normalization, Figures 4-47 and 4-48 have been prepared. These plot heat rate data from Day 1 against torque and against timing, respectively. These figures show clear (and expected) monotonic relationships – higher torque and more advanced timing led to lower heat rate. It should be possible to fit regression lines to these data and extrapolate with reasonable accuracy from the torques at which data was obtained on Day 1 to the 101 and 102% values at which data was obtained in February, and to do this for timing values which match. This has not yet been undertaken at this stage in the analysis, but will be completed in the near future. Thus, the conclusions section will be somewhat qualitative – the generally

beneficial influence of the modifications is clear, but the specific numerical comparison will be the subject of further analysis.

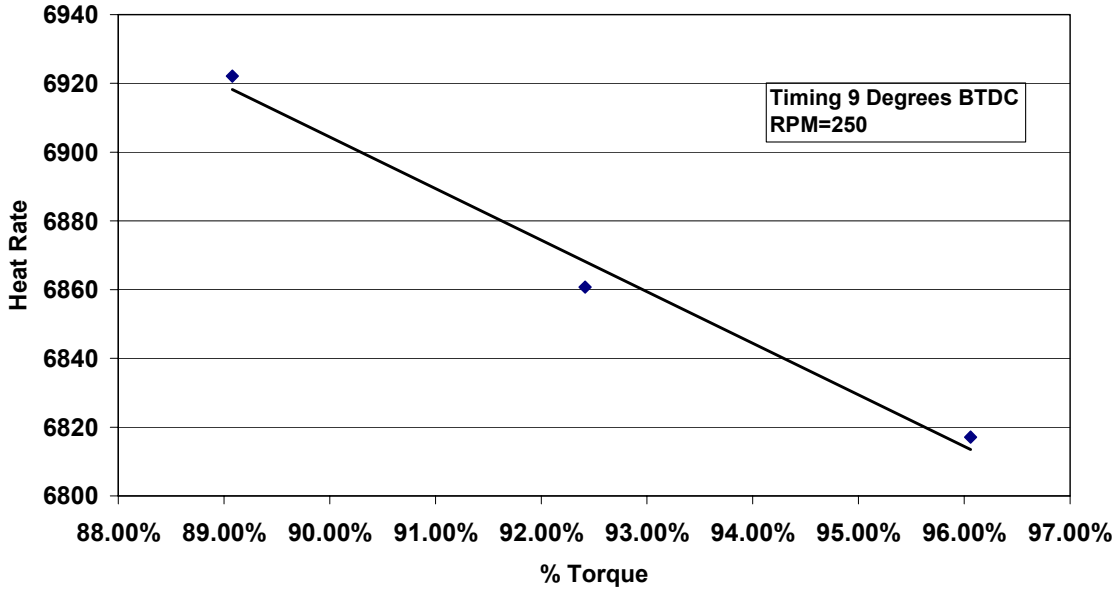

Figure 4-47. Heat Rate *versus* Unit Torque; Day 1; Unit 6; After Modification; Williams' Station 60; August 25, 2004

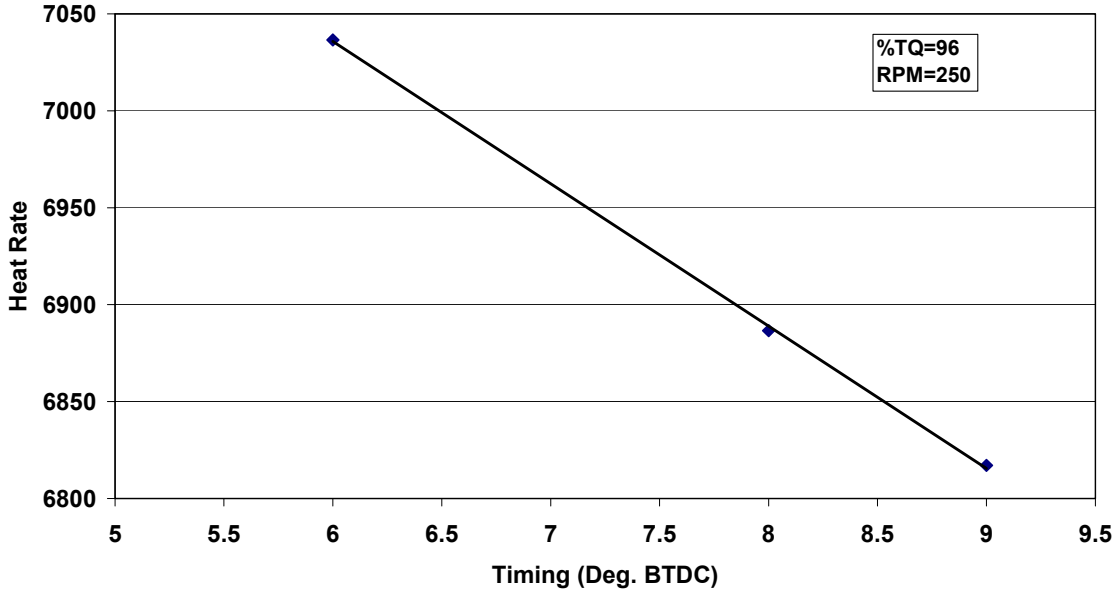

Figure 4-48. Heat Rate *versus* Timing; Day 1; Unit 6; After Modification; Williams' Station 60; August 25, 2004

In addition to the variation of heat rate with torque and timing, operational decisions need to consider how to optimize overall system efficiency and in some cases to superimpose an emissions constraint.

Figure 4-49 shows the variation of system thermal efficiency with torque. This is not such a clear monotonic relationship, and shows a maximum value for system thermal efficiency at 92% torque, because at the higher torque, there is some influence of the unloader arrangement (which may in turn influence pulsations). The difference between the value at 92% and 96% torque is less than 0.2% in system efficiency, but makes the point that heat rate alone should not be the total consideration in mapping performance for operational decision making.

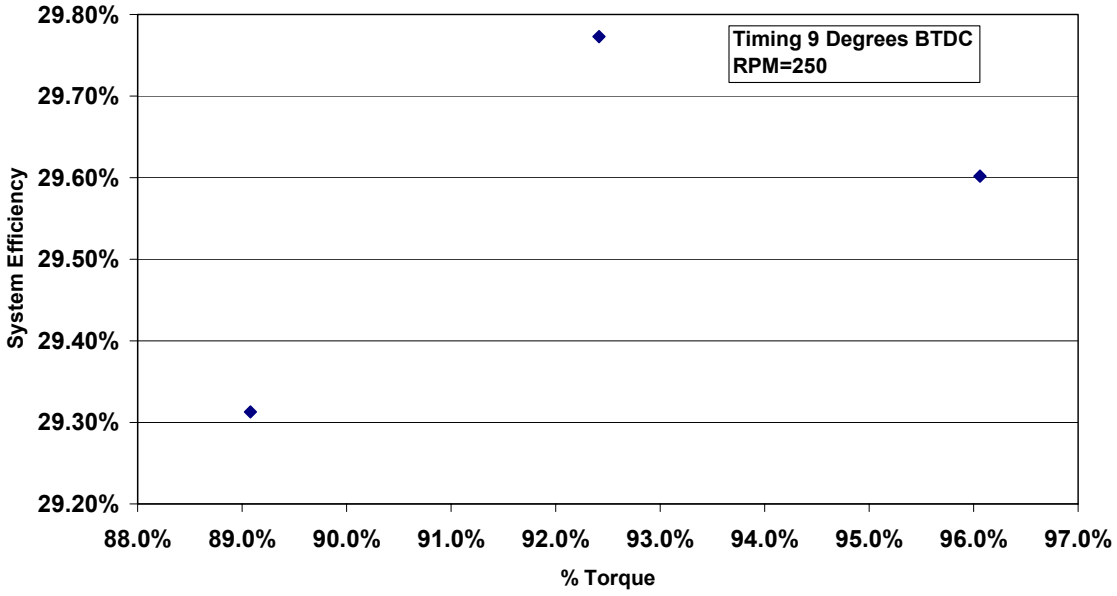

Figure 4-49. System Efficiency *versus* Unit Torque; Day 1; Unit 6; After Modification; Williams' Station 60; August 25, 2004

5. RESULTS AND DISCUSSION: AIR BALANCE TASKS

The work completed on the Air Balance task this quarter include the following:

- Testing of the GMVH engine in a pre-chamber configuration to acquire simulation data is completed and data being processed.

- Significant effort expended trying to get simulation model validated. Optimum Power Technology (OPT) software has been revised several times. SwRI personnel visited OPT on October 5-7, 2004 for a coordinated effort to revise software and GMVH model for more accurate simulation.

- GMVH engine has been partially disassembled to allow for detailed geometric analysis. Detailed geometry required for accurate simulation and to investigate variability of compression ratio and port timings amongst cylinders.

- Two of the six cylinders have been removed for flowbench testing. Flowbench testing is required to get accurate port discharge coefficient data for simulation. Testing of high and low compression pressure (presumed high and low airflow) cylinders on the same bank is required to determine the variability and contribution to airflow imbalance.

- A TOC Review meeting held at SwRI on September 14, 2004. A follow-up meeting was held at the Gas Machinery Conference on October 3, 2004.

Engine testing involved operation in both open chamber and pre-chamber configurations. The majority of two-stroke integral engines operate in the open chamber configuration. Thus, testing was conducted to acquire baseline performance and emissions data. The combustion variability is typically quite high with open chamber combustion systems. Therefore, testing in a pre-chamber configuration, where combustion stability is much improved, was conducted to acquire more repeatable data for simulation.

The engine testing was conducted over engine speeds of 231, 264, 297, and 330 RPM. Engine load was also varied from 70, 85, 90, and 100 of rated. Within this map of engine speed and load, the air/fuel ratio and spark timing was varied. In analyzing the data, the spread of compression pressures was seen to remain very consistent regardless of the operating condition. This consistency is shown in Figure 5-1, where the pressure at 20 degrees before top dead center for all cylinders at all operating conditions tested is plotted *versus* air manifold pressure.

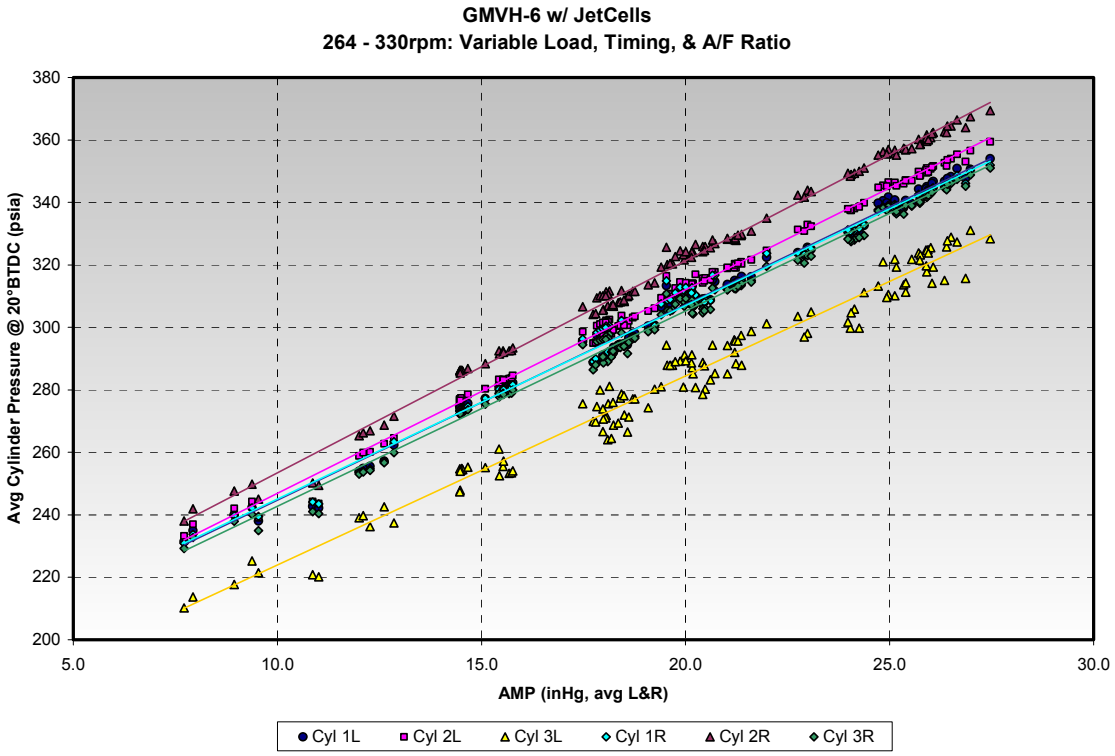

Figure 5-1. Comparison of Cylinder-to-Cylinder Compression Pressure at All Operating Conditions

In the *Engine Simulation* subtask, a significant amount of work has been invested in creating a geometric model and characteristics of combustion and turbocharger for the GMVH-6 engine. The baseline test data has been analyzed for characterizing the combustion and engine performance. Data provided by Cooper on the turbocharger and measurements on the test engine were analyzed to create detailed maps of compressor and turbine performance. Drawings and external geometric measurements on the test engine were compiled to model the complex

geometry of manifolds, ports, and cylinders. A schematic of the engine model is depicted in Figure 5-2.

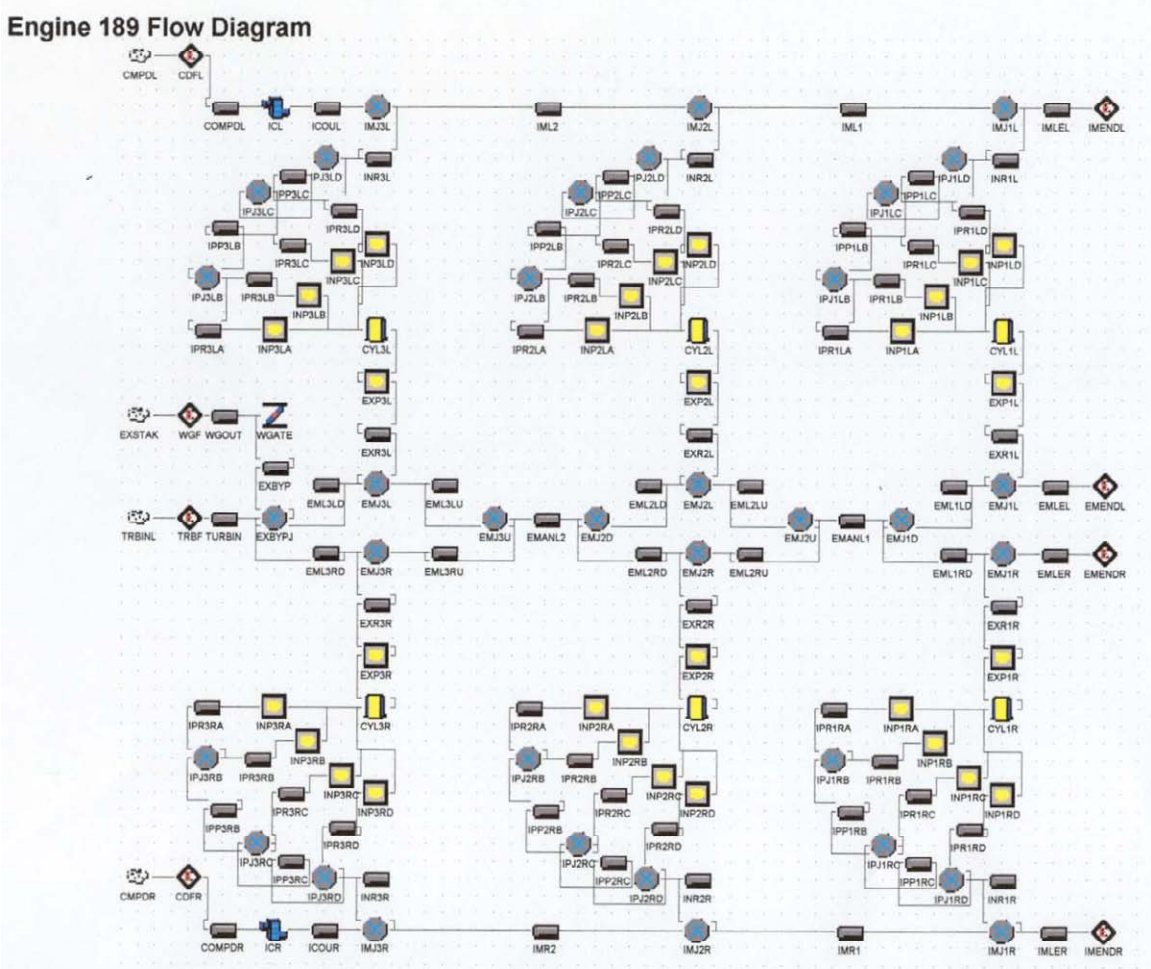

Figure 5-2. Schematic of GMVH-6 Engine Model

Several iterations of the software have been compiled to address the specifics of the GMVH engine. The latest simulations have predicted mass airflow closely, but have not accurately predicted the amplitude and phasing of pulsations in the inlet and exhaust manifolds. It is believed that the inaccurate manifold dynamic predictions may be due to the use of inaccurate discharge coefficients and inaccurate representations of the complicated cylinder plenum geometry that could not be measured externally. Geometric measurements and flow testing, as described below, should allow improved simulation of the test engine.

During the model creation, drawings provided by Cooper of engine components were used to create the engine geometry. The drawing for the cylinders showed an allowable casting variation for the exhaust ports, as depicted in Figure 5-3. This allowable variation, coupled with a current inability to accurately simulate dynamic pulsations, led to concerns that the true port geometry as exists on the test engine was not being properly modeled, and that the air imbalance may be more affected by port flow variation than originally assumed. Thus, it was determined that the only correct course of action was to disassemble the test engine and measure the geometric and flow differences between cylinders.

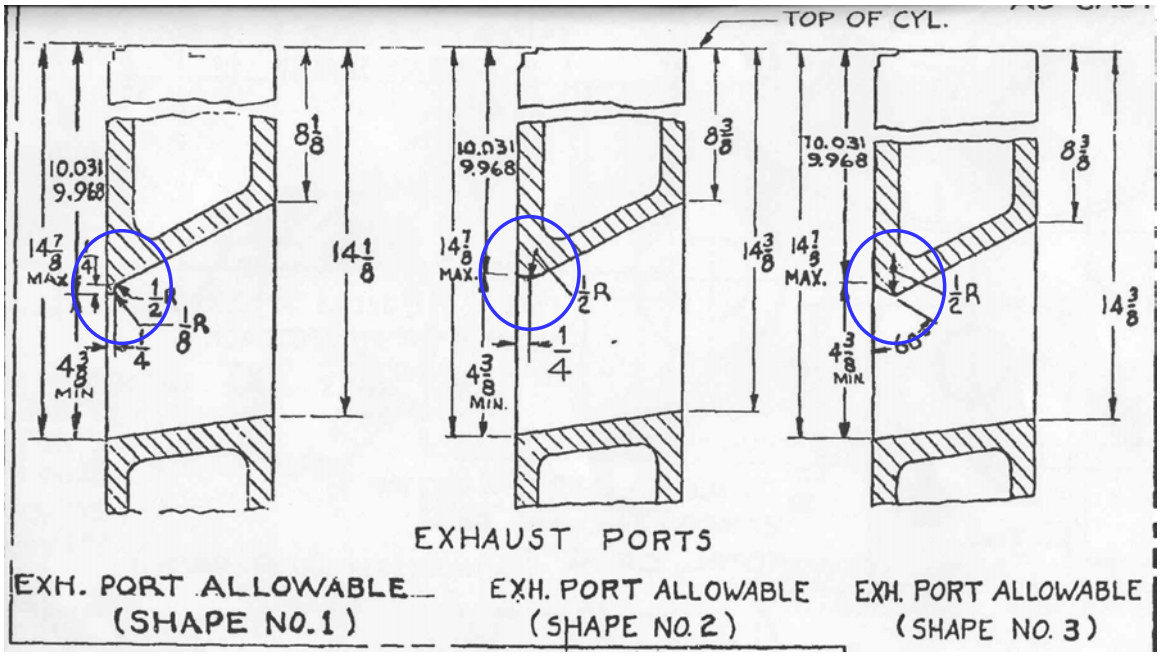

Figure 5-3. Allowable Exhaust Port Geometry

The test engine has been disassembled and a geometric analysis is currently in progress. The geometric analysis involves many detailed measurements on all cylinders to quantify the variation cylinder-to-cylinder in compression ratio, inlet and exhaust port timing, and inlet and exhaust port geometry. Cylinders 1left and 3left were removed from the engine to be flow tested. Flow testing will be performed to: first, obtain accurate discharge coefficient data for modeling and, secondly, to determine the variation between a high (1left) and low (3left) compression pressure cylinder from the same bank.

The flow bench testing will involve a test rig being constructed to flow air across the ports at prescribed pressure ratios. Several measurements will be taken at different pressure ratios and port openings. The test rig will allow for setting piston height to set a prescribed opening area. Flow nozzles will be installed in a meter run from a compressor to measure the airflow for discharge coefficient calculation.

The results from the geometric analysis and flow bench testing will be utilized in the engine model to obtain more accurate simulations. The model will then be utilized to investigate the affects on cylinder-to-cylinder air balance from not only manifold design, but also the potential variation in compression ratio and port flow that likely exists in all two-stroke integral engines. It is important to quantify the variation and affects of these geometric parameters, because their significance in terms of air balance may change the path taken for manifold design and the potential benefit of manifold design modifications.

6. CONCLUSIONS

1. Modifications to Unit 1 GMW10 to add high-pressure fuel injection and a turbocharger achieved a significant reduction in heat rate and NOx concentration; crankshaft strain was also reduced by a small amount.

2. As on other engines, retarding timing was shown to increase heat rate and NOx on this GMW10.

3. Retarding timing also decreased strain.

4. Combustion pressure ratio balancing was successfully demonstrated again, but with little or no observable benefit to heat rate for either PFP or CPR balancing.

5. The influence of both CPR and PFP balancing did have a notable effect in reducing crankshaft strain; this may have been that the rich cylinder in the unbalanced condition had its peak-firing pressure reduced.

6. The self-powered rod load monitor had its most successful demonstration so far. Its inferred power based on measured strain, Young's modulus, and rod diameter were within 0.9% to 2.6% of indicated power.

7. System thermal efficiency of 29 to 30% was observed at 250 RPM, as compared to 27 to 27.5 for the unmodified unit.

8. Reducing speed from 250 RPM reduced overall system efficiency substantially because of an auto-retard in timing, and because of reduction in compressor efficiency. It also tended to increase measured crankshaft strain for the conditions observed.

7. REFERENCES

[1] Smalley, A.J., Mauney, D.A., and Ash, D.I., (1997) Final Report PR-15-9529, "Compressor Station Maintenance Cost Analysis," prepared for the Compressor Research Supervisory Committee of PRC *I*nternational, SwRI Project No. 04-7424.

[2] McKee, R.J., Smalley, A.J., Bourn, G.D., and Young, K.N., (2003) "Detecting Deterioration of Compression Equipment by Normalizing Measured Performance Relative to Expected Performance," GMRC Gas Machinery Conference (GMC), Salt Lake City, Utah.

[3] Harris, R.E., Edlund, C.E., Smalley, A.J., and Weilbacher, G., (2000) "Dynamic Crank Web Strain Measurements for Reciprocating Compressors," presented at the GMRC Gas Machinery Conference (GMC), Colorado Springs, Colorado.

8. LIST OF ACRONYMS AND ABBREVIATIONS

AGA3	Gas Flow Measurement Standard
BEI	Manufacturer's Trade Name
BHP	Brake Horsepower
BTDC	Before Top Dead Center
BTU	British Thermal Unit
CES	Cooper Energy Services
COV	Coefficient of Variance
CPR	Compression Pressure Ratio
DAS	Data Acquisition System
DOE	U.S. Department of Energy
GMC	Gas Machinery Conference
GMRC	Gas Machinery Research Council
GMVH	Cooper Engine Model
GMVH6	Cooper Engine Model with Six Power Cylinders
GMW10	Cooper Engine Model with Ten Power Cylinders
HBA-6T	Clark Engine Model with Six Power Cylinders
HP	Horsepower
IAC	Industry Advisory Committee
IRV	Instantaneous Rotational Velocity
LHV	Lower Heating Value
NGK	Manufacturer's Trade Name
NOx	Oxides of Nitrogen
OPT	Optimum Power Technology
PCB	Manufacturer's Trade Name
PFP	Peak-Firing Pressure
PSI	Pounds Per Square Inch
RLM	Rod Load Monitor
RPM	Revolutions Per Minute
SCF	Standard Cubic Feet
SDCM	Strain Data Capture Module
SwRI®	Southwest Research Institute®
TCF	Trillion Cubic Feet
TDC	Top Dead Center
TLA6	Clark Engine Model with Six Power Cylinders
UEGO	Universal Exhaust Gas Oxygen
V-10	10-Cylinder Engine with V Configuration